Temporal control of PDGFRα regulates the fibroblast-to-myofibroblast transition in wound healing

Longbiao Yao[1], Bharath H. Rathnakar[1], Hae Ryong Kwon[1], Hiromi Sakashita[1], Jang H. Kim[1,2], Alex Rackley[1], James J. Tomasek[2], William L. Berry[3], Lorin E. Olson[1,2,4,*]

[1]Cardiovascular Biology Research Program, Oklahoma Medical Research Foundation, Oklahoma City, OK 73104, USA

[2]Department of Cell Biology, University of Oklahoma Health Sciences Center, Oklahoma City, OK 73104, USA

[3]Department of Surgery, University of Oklahoma Health Sciences Center, Oklahoma City, OK 73104, USA

[4]Lead contact

SUMMARY

Fibroblasts differentiate into myofibroblasts by acquiring new contractile function. This is important for tissue repair, but it also contributes to organ fibrosis. Platelet-derived growth factor (PDGF) promotes tissue repair and fibrosis, but the relationship between PDGF and myofibroblasts is unclear. Using mice with lineage tracing linked to PDGF receptor α (PDGFRα) gene mutations, we examine cell fates during skin wound healing. Elevated PDGFRα signaling increases proliferation but unexpectedly delays the fibroblast-to-myofibroblast transition, suggesting that PDGFRα must be downregulated for myofibroblast differentiation. In contrast, deletion of PDGFRα decreases proliferation and myofibroblast differentiation by reducing serum response factor (SRF) nuclear localization. Consequences of SRF deletion resemble PDGFRα deletion, but deletion of two SRF coactivators, MRTFA and MRTFB, specifically eliminates myofibroblasts. Our findings suggest a scenario where PDGFRα signaling initially supports proliferation of fibroblast progenitors to expand their number during early wound healing but, later, PDGFRα downregulation facilitates fibroblast differentiation into myofibroblasts.

In brief

Yao et al. use lineage-tracing and wound-healing experiments in mice to investigate functions of the PDGFRα signaling pathway in the fibroblast-to-myofibroblast transition. Their analysis indicates an early role for PDGFRα-SRF signaling to support fibroblast proliferation, followed by PDGFRα downregulation and a transition to MRTF-SRF control over myofibroblast differentiation.

Graphical Abstract
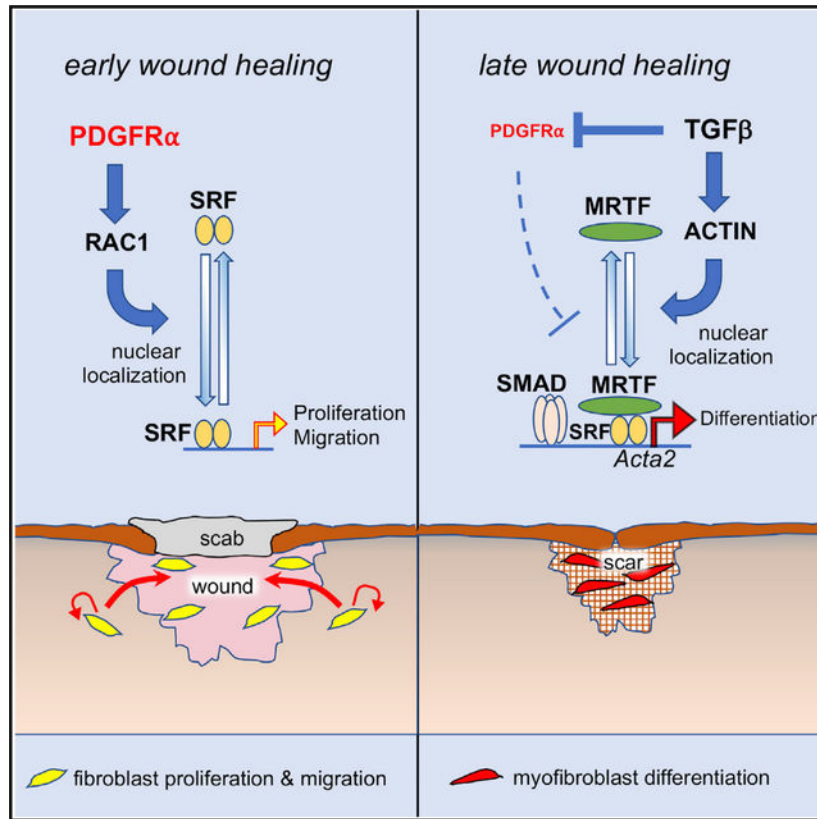
INTRODUCTION

Most organs possess the ability to respond to tissue injury by forming scar tissue. In this process, fibroblastic progenitor cells proliferate and secrete extracellular matrix (ECM) before differentiating into contractile myofibroblasts (Plikus et al., 2021; Soliman et al., 2021). The myofibroblasts acquire force-generating properties through *de novo* expression of alpha smooth muscle actin (αSMA) and other proteins normally found in smooth muscle cells (Hinz, 2007; Tomasek et al., 2002). Transient myofibroblasts in wound healing are beneficial because their contraction reduces the size of the tissue defect needing to be plugged by scar tissue (Gurtner et al., 2008), but persistence of myofibroblasts leads to fibrosis that creates a significant clinical burden (Henderson et al., 2020).

The principal source of myofibroblasts in wound healing is local fibroblastic progenitors, sometimes called fibro-adipogenic progenitors because of their dual potential for fibrogenic

and adipogenic differentiation (Driskell et al., 2013; Guerrero-Juarez et al., 2019; Joe et al., 2010; Kanisicak et al., 2016; Rinkevich et al., 2015; Shook et al., 2018; Uezumi et al., 2011). Progenitors become activated by cytokines and growth factors released from platelets and infiltrating leukocytes (Werner and Grose, 2003). Among these signals, platelet-derived growth factor (PDGF) has a key role driving proliferation and migration (Beer et al., 1997; Greenhalgh et al., 1990). From lineage-tracing studies in mice, it is known that many PDGF-activated progenitors differentiate into αSMA[+] myofibroblasts (Li et al., 2018; Shook et al., 2018). This leads to an expectation that PDGF promotes, and might be required for, myofibroblast differentiation. The myofibroblast phenotype largely depends on the transcriptional activity of serum response factor (SRF), which is constitutively localized to the nucleus. Extracellular signals and matrix stiffness enhance SRF activity through two coactivators, MRTFA and MRTFB, which shuttle in and out of the nucleus depending on actin polymerization (Pipes et al., 2006). SRF and myocardin-related transcription factors (MRTFs) are required for transforming growth factor β (TGF-β) to induce fibroblast-to-myofibroblast transitions (Crider et al., 2011; Davis et al., 2015), and pharmacological activation of MRTFs enhances myofibroblast differentiation in wound healing (Velasquez et al., 2013). SRF directly regulates two distinct genetic programs driving proliferation or myofibroblast differentiation (Gualdrini et al., 2016; Miano, 2003). As an upstream signal, PDGFRα regulates SRF and MRTF during neural crest development (Dinsmore and Soriano, 2022; Vasudevan and Soriano, 2014), but whether PDGFRα engages SRF and MRTF to regulate myofibroblast differentiation has not been investigated.

PDGF binds to tyrosine kinase receptors on the cell surface, composed of PDGFRα and/or PDGFRβ, which induces receptor dimerization and kinase activation. Autophosphorylated tyrosines on the receptor cytoplasmic region then serve as binding sites for the effectors of downstream signaling pathways including PI3K, ERK, PLCγ, and STATs (Andrae et al., 2008; Heldin and Westermark, 1999; Hoch and Soriano, 2003). PDGFRα and PDGFRβ are expressed on fibroblasts in most adult organs at homeostasis (Muhl et al., 2020). Of particular interest, organ fibrosis develops spontaneously (without injury) in mice with a D849V knockin mutation in PDGFRα (Olson and Soriano, 2009). This mutation, also called the K (kinase domain) mutation, impairs autoinhibitory functions of the kinase domain and allows constitutive signaling to occur. PDGFRα[K]-driven fibrosis involves altered cell fate, where fibroblastic progenitors become activated fibroblasts that produce collagen at the expense of adipogenic potential (Iwayama et al., 2015; Sun et al., 2017). Whether these PDGFRα[K]-activated fibroblasts progress to become contractile myofibroblasts is unknown.

Given that PDGFRα signaling is critical for wound repair and the appearance of myofibroblasts is critical for wound closure, we aimed to resolve the relationship between PDGFRα and myofibroblasts. Do PDGFRα[K]-activated cells spontaneously differentiate into αSMA[+] myofibroblasts? How does the loss of PDGFRα affect the fibroblast-to-myofibroblast transition? What is the functional relationship between PDGFRα, SRF, and MRTFs? Our results show that the temporal control of PDGFRα signaling regulates the transition from proliferating progenitor to contractile myofibroblast. Elevated PDGFRα signaling increases proliferation but delays the emergence of αSMA[+] myofibroblasts from activated fibroblasts. On the other hand, deletion of *Pdgfra* decreases proliferation and formation of activated fibroblast progenitors, as well as myofibroblast differentiation, which

is accompanied by loss of Rac1 activity and SRF nuclear localization. Finally, similar to *Pdgfra* deletion, *Srf* deletion decreases proliferation and myofibroblast differentiation, but double deletion of *Mrtfa* and *Mrtfb* specifically causes a loss of αSMA$^+$ myofibroblasts without affecting proliferation and formation of activated fibroblast progenitors. These phenotypes suggest that PDGFRα has overlapping functions with SRF in control of proliferation and migration, but PDGFRα has distinct functions from SRF and MRTFs in myofibroblast differentiation.

RESULTS

PDGFRα^K impairs dermal wound healing

To investigate the consequence of elevated PDGFRα signaling in tissue repair, we performed wound-healing studies on *Ubc-Pdgfra$^{Flp/+}$* control mice and *Ubc-Pdgfra$^{K/+}$* mice with constitutively active PDGFRα. *Ubc-Pdgfra$^{Flp/+}$* mice have a lox-PDGFRα:STOP-lox-Flp° cassette inserted at *Pdgfra*, along with *UbcCreER^{tg}* and *Rosa26$^{FSF-tdTomato}$* alleles. In these mice, Tmx induces deletion of a floxed cassette to allow Flp° expression in PDGFRα$^+$ cells (Figure 1A). *Ubc-Pdgfra$^{K/+}$* mice have a lox-STOP-lox-PDGFRαK-T2A-Flp° cassette inserted at *Pdgfra*, plus *UbcCreER^{tg}* and *Rosa26$^{FSF-tdTomato}$*. In these mice, Tmx induces deletion of a floxed cassette to allow expression of PDGFRα^K together with Flp° (Figure 1B). In both models, *Pdgfra*-derived cells express Tomato based on the intersection of global *Ubc*-driven Cre and fibroblast *Pdgfra*-driven Flp (Sun et al., 2020). Tomato is not expressed in the absence of Tmx (Figures S1A and S1B). We chose globally active *UbcCreER* because our goal is to target and track any cell that expresses *Pdgfra* in tissue repair. Recent studies have identified unexpected progenitor sources for myofibroblasts, including adipocytes and myeloid cells, that acquire *Pdgfra* expression only when recruited to the wound site (Guerrero-Juarez et al., 2019; Shook et al., 2020). Using a "fibroblast-specific" Cre (e.g., *Pdgfra-CreER*) would exclude these progenitors and would be redundant with *Pdgfra$^{K.Flp/+}$* and *Pdgfra$^{Flp/+}$* as knockin alleles of *Pdgfra*. We administered Tmx three times (days −9, −7, and −5), created wounds on day 0, and then excised wounds and surrounding skin at day +7 (Figure 1C). We used histomorphometry on the wound center (Figure 1D) to measure three wound features: wound bed cross-sectional area, wound contraction as a percentage of the original 5 mm width (a lower percentage indicates more contraction), and epithelialization, which means the percentage of the wound surface covered by newly generated epidermis (a higher percentage indicates more epithelialization). *Ubc-Pdgfra$^{K/+}$* wound beds display a significantly larger cross-sectional area (Figure 1E) and retain most of their original size at day 7, whereas control wounds contract to ~50% of the original size (Figure 1F). Only 3/8 *Ubc-Pdgfra$^{K/+}$* wounds completely epithelialize by day 7, compared with 8/8 *Ubc-Pdgfra$^{Flp/+}$* wounds (Figure 1G). In both genotypes, PDGFRα is expressed in granulation tissue (Figure S1C). Collagen, the most abundant ECM in the dermis and granulation tissue, and periostin, a matricellular protein secreted by myofibroblasts, are both reduced in *Ubc-Pdgfra$^{K/+}$* wounds compared with *Pdgfra$^{Flp/+}$* (Figures S1D and S1E). Therefore, elevated PDGFRα signaling leads to defective wound healing by day 7 rather than improved healing.

PDGFRα^K enhances proliferation but delays myofibroblast differentiation

We used the $Rosa26^{FSF\text{-}tdTomato}$ reporter to assess proliferation, migration, and differentiation of $Pdgfra$-derived cells. By EdU incorporation in day 4 wounds, we observe that $Pdgfra^K$-derived Tomato$^+$ cells in mutant wounds are significantly more proliferative than Tomato$^+$ cells in control wounds (Figures 1H and 1I). The location of Tomato$^+$ cells at day 7 verifies that both genotypes contain Tomato$^+$ cells distributed throughout the granulation tissue, but the $Ubc\text{-}Pdgfra^{K/+}$ wounds clearly contain more Tomato$^+$ cells (Figure 1J). Therefore, elevated PDGFRα signaling enhances progenitor proliferation and migration, in agreement with previous work showing that $Pdgfra^{K/+}$ embryonic fibroblasts were more proliferative and more migratory (Olson and Soriano, 2009).

In $Ubc\text{-}Pdgfra^{K/+}$ wounds, αSMA$^+$ cells are densely clustered at the wound perimeter and center, with intervening areas lacking αSMA (Figure 1K). The area of αSMA stain is significantly lower in $Ubc\text{-}Pdgfra^{K/+}$ wounds (Figure 1L). More specifically, in $Ubc\text{-}Pdgfra^{K/+}$ wounds, areas with the most αSMA$^+$ cells are anti-correlated with Tomato$^+$ cells (arrowheads in Figures 1K and 1L). We verified anti-correlation of these markers at the individual cell level by calculating the myofibroblast index of αSMA expression in Tomato$^+$ cells. Indeed, differentiation of $Pdgfra^K$-derived progenitors into αSMA$^+$ myofibroblasts is severely reduced at day 7 (Figures 1M and 1N). By day 10, however, complete epithelialization is achieved in $Ubc\text{-}Pdgfra^{K/+}$ wounds, and myofibroblast indices are similar between $Ubc\text{-}Pdgfra^{Flp/+}$ and $Ubc\text{-}Pdgfra^{K/+}$ wounds (Figures S1F–S1H). This indicates that the myofibroblast deficiency induced by PDGFRα^K is temporary. Together, these results show that PDGFRα^K produces abundant new tissue through increased cell proliferation and migration, but these cells exhibit delayed fibroblast-to-myofibroblast transition during the first week of healing.

PDGFRα^K-driven fibrosis does not involve myofibroblasts

Myofibroblasts are not found in most tissues at homeostasis, but they appear in wound healing and many fibrotic diseases because of pro-myofibroblast signals (e.g., TGF-β) and mechanical forces that are not present in healthy tissue. PDGFRα^K drives spontaneous fibrosis in the skin and other organs (Olson and Soriano, 2009), but whether this induces αSMA$^+$ myofibroblasts is unclear. To investigate, we administered Tmx to 10-day-old $Ubc\text{-}Pdgfra^{K/+}$ mutant pups and $Ubc\text{-}Pdgfra^{+/+}$ littermates and sacrificed them 5 months later to analyze fibrosis in skin, intestine, subcutaneous fat, and skeletal muscle (Figures S2A and S2B). In each organ, trichrome stain confirms fibrotic deposits in mutant tissues that are absent from controls (Figures S2C–S2F). Fibrotic regions contain high cell density with Tomato labeling but no ectopic αSMA. These results suggest that PDGFRα^K signaling in uninjured tissue drives fibrosis without converting progenitors into myofibroblasts.

Opposing functions of PDGFRα^K and TGF-β on myofibroblast differentiation

To examine the ability of PDGFRα^K-expressing cells to differentiate and function as myofibroblasts *in vitro*, we isolated primary dermal fibroblasts (DF) from $Pdgfra^{+/+}$ and $Pdgfra^{K/+}$ mice. We tested contractile function by suspending DFs in collagen lattices attached to tissue culture plastic and induced myofibroblast differentiation by treating with 10% serum for 4 days. Mitomycin C was included to control for proliferation differences.

Upon release from the plastic, $Pdgfra^{+/+}$ DFs contract strongly, reducing the lattice to 30% of the original size, but $Pdgfra^{K/+}$ DFs contract poorly, achieving only 60% of original size (Figure 2A). $Pdgfra^{K/+}$ DFs also contract poorly when treated with TGF-β1 (Figure 2A). Under growth conditions, morphological differences are obvious in that $Pdgfra^{K/+}$ DFs are smaller and exhibit lower αSMA expression than $Pdgfra^{+/+}$ cells (Figures 2B and 2E).

TGF-β1 induces myofibroblast differentiation through the action of SMAD2/3 transcription factors, MRTFs, and p38 kinases (Crider et al., 2011; Hinz, 2007; Meyer-Ter-Vehn et al., 2006). To more closely examine the TGF-β1 response, we serum starved $Pdgfra^{+/+}$ and $Pdgfra^{K/+}$ DFs and then treated them with TGF-β1. In response, αSMA is upregulated from 0 to 12 h of treatment in both genotypes. Increased αSMA is coordinated with downregulation of PDGFRα, and both responses are delayed in $Pdgfra^{K/+}$ DFs (Figure 2C). TGF-β1 induces similar SMAD3 phosphorylation in both cell genotypes (Figure 2C). Reciprocal changes are also seen at the level of $Pdgfra$ and $Acta2$ (αSMA) mRNA in TGF-β1-treated $Pdgfra^{+/+}$ cells (Figure 2D).

To investigate transcriptional regulators of myofibroblast differentiation in $Pdgfra^{K/+}$ DFs, we examined SRF, MRTFA, and MRTFB. Surprisingly, MRTFA and MRTFB are upregulated in $Pdgfra^{K/+}$ DFs compared with in $Pdgfra^{+/+}$, and SRF expression is normal (Figure 2E). MRTFA and MRTFB accumulate in the nucleus of serum-treated cells of both genotypes (Figure 2F), suggesting that SRF-MRTF signaling is functional in $Pdgfra^{K/+}$ DFs. This is surprising because SRFs and MRTFs should strongly promote myofibroblast differentiation (Crider et al., 2011; Davis et al., 2015; Small et al., 2010). Therefore, although the molecular mechanisms by which PDGFRα opposes myofibroblast differentiation are still unclear, these results argue against defective TGF-β-SMAD or SRF-MRTF signaling. Moreover, these results show that PDGFRα and TGF-β exert opposing influences on the fibroblast-to-myofibroblast transition, with TGF-β having the ability to downregulate PDGFRα^K in DFs during myofibroblast differentiation (Figure 2G).

Pdgfrα is downregulated in myofibroblasts and is not required for their maintenance

The ability of TGF-β1 to downregulate PDGFRα suggests that PDGFRα might not be critical for later stages of wound healing after myofibroblast differentiation. We observed marked downregulation of $Pdgfra^{H2BGFP}$ in day 7 wounds compared with adjacent unwounded dermis (Figure S3A). This is consistent with downregulation of $Pdgfra^{H2BGFP}$ in fibro-adipogenic progenitors in injured versus uninjured skeletal muscle (Contreras et al., 2019). Immunofluorescence for PDGFRα and αSMA also demonstrates significant downregulation of PDGFRα from day 5 to day 7, alongside upregulation of αSMA expression (Figures S3B and S3C). Similar patterns are observed at the mRNA level, with $Pdgfra$ trending down alongside upregulation of $Acta2$ and $Postn$ (Figure S3D).

To test PDGFRα function in myofibroblasts, we used $Postn^{MerCreMer}$, a Tmx-regulated Cre active in myofibroblasts but not in progenitors (Bugg et al., 2022; Kanisicak et al., 2016). We verified Cre activity in the skin by creating wounds in $Postn^{MerCreMer}$;$ROSA26^{LSL-Tomato}$;$Col1a1-GFP$ reporter mice and then administering Tmx after wounding. GFP is expressed in unwounded dermis and wound tissue. However, Tomato$^+$ cells are sparse in unwounded dermis and abundant in the wound bed, consistent

with labeling myofibroblasts specifically (Figure S3E). Tomato is only seen in wounds with Tmx (Figure S3F). Interestingly, when wounds are mounted flat and sectioned in the plane of the skin, Tomato$^+$ cells form a cell-dense ring around the margin of the wound bed with a lower density of labeled cells in the wound center (Figure S3G). This pattern suggests that myofibroblasts localize to the wound edges on days 5–6 before coalescing into the wound center during tissue contraction. Next, we generated myofibroblast *Pdgfra* controls and knockouts (controls: *Postn-Pdgfra*$^{Flp/+}$; knockouts: *Postn-Pdgfra*$^{Flp/Flp}$), and *Pdgfra*$^{K/+}$ mice, with *Postn*^{MerCreMer} (Figures 3A–3D). By day 7, the wounds of all mice were similar in area, contraction, and epithelialization (Figures 3E–3H). In this experiment, sequential intersection of *Postn*-driven Cre and *Pdgfra*-driven Flp mediates activation of a Flp-dependent reporter. However, Tomato$^+$ cells are not detected in any of the genotypes (Figure 3I), consistent with downregulation of *Pdgfra* in *Postn*$^+$ myofibroblasts. αSMA$^+$ myofibroblast are localized to the wound center in all genotypes (Figure 3J). We verified Cre-mediated recombination of the *Pdgfra* loci by PCR genotyping of *Postn-Pdgfra*$^{Flp/+}$ and *Pdgfra*$^{K/+}$ wounds (Figures 3K and 3L).

To confirm the functionality of *Postn*^{MCM} for gene deletion in myofibroblasts, we combined it with *Mrtfa*$^{-/-}$;*Mrtfb*$^{flox/flox}$ mice (Mokalled et al., 2010) to generate myofibroblast *Mrtfa/Mrtfb* knockouts (*Postn-Mrtfa*$^{-/-}$*b*$^{flox/flox}$). Controls were mice without *Postn*^{MCM} or *Mrtfa*$^{+/-}$ (both denoted as *Mrtfab*^{control}) (Figures S4A–S4C). At day 7, knockout wounds are poorly contracted with incomplete epithelialization (Figures S4D–S4G). Tomato is expressed in both genotypes, albeit reduced in *Postn-Mrtfa*$^{-/-}$*b*$^{flox/flox}$ wounds (Figure S4H). The αSMA$^+$ area is significantly lower *in Postn-Mrtfa*$^{-/-}$*b*$^{flox/flox}$ wounds compared with controls (Figures S4I and S4J), and specific to the Postn-derived Tomato$^+$ population, a majority are αSMA$^+$ in controls, but this overlap is severely reduced in *Postn-Mrtfa*$^{-/-}$*b*$^{flox/flox}$ wounds (Figures S4K and S4L). These results show that *Postn*^{MCM} is effective for gene deletion in dermal myofibroblasts and that MRTFs are critical for sustaining myofibroblasts, as expected (Crider et al., 2011).

Progenitor proliferation and myofibroblast differentiation require PDGFRα

To investigate how *Pdgfra* knockout affects wound healing, we generated conditional *Pdgfra* knockout mice (*Ubc-Pdgfra*$^{Flp/Flp}$) with *Ubc-Pdgfra*$^{Flp/+}$ littermates as controls (Figures 4A–4C). Immunohistochemistry confirms the absence of PDGFRα in *Ubc-Pdgfra*$^{Flp/Flp}$ wounds (Figure S5A). *Ubc-Pdgfra*$^{Flp/Flp}$ wounds display a larger cross-sectional area and retain most of their original width at day 7 compared with control wound beds (Figures 4D–4F). In half of the *Ubc-Pdgfra*$^{Flp/Flp}$ wounds, there is delayed epithelialization, with epithelial tongues migrating down into the wound bed (Figures 4G and 4D, arrowheads), creating an open gap beneath the attached eschar (Figure 4D, asterisk). Collagen and periostin are reduced in *Ubc-Pdgfra*$^{Flp/Flp}$ granulation tissue (Figures S5B and S5C). Proliferation is significantly reduced in *Ubc-Pdgfra*$^{Flp/Flp}$ wounds at day 4 (Figures 4H and 4I). In control wounds at day 7, αSMA$^+$ myofibroblasts and Tomato$^+$ cells migrate to the center of the granulation tissue. But in *Ubc-Pdgfra*$^{Flp/Flp}$ wounds, myofibroblasts localize to the wound edges, and Tomato$^+$ cells are sparse (Figures 4J and 4K). The area of αSMA stain and the percentage of Tomato$^+$ cells with αSMA are both significantly lower in *Ubc-Pdgfra*$^{Flp/Flp}$ wounds (Figures 1L–1N).

Therefore, progenitor cells lacking *Pdgfra* are less proliferative and resist myofibroblast differentiation during wound healing.

PDGFRα and RAC1 regulate SRF nuclear localization

We noted that SRF is markedly more cytoplasmic in *Ubc-Pdgfra$^{Flp/Flp}$* wounds compared with its predominantly nuclear localization in wound tissue from *Ubc-Pdgfra$^{Flp/+}$* mice (Figures S5D and S5E). Reduced myofibroblast differentiation in *Pdgfra*-deficient wounds may be due to the lack of appropriate signaling needed for SRF activity. NIH/3T3 fibroblasts express PDGFRα and are a well-characterized model to investigate how SRF regulates genetic programs governing proliferation and contraction (Esnault et al., 2014; Hill et al., 1995). We used CRISPR-Cas9 to create *Pdgfra$^{CRISPR-KO}$* 3T3 cells. Knockout cells (aR-KO) do not activate signaling cascades or gene expression in response to PDGF-AA, but they retain low levels of PDGFRβ and respond weakly to PDGF-BB (Figures 5A, S6A, and S6B). In the presence of serum, which contains PDGF as one of its major growth factors, aR-KO cells exhibit a rounded morphology with less F-actin and αSMA (Figures 5B and S6C). Transcripts for *Srf* and *Acta2* are low in aR-KO cells (Figure S6D), but SRF protein levels are still similar between 3T3 and aR-KO cells (Figure 5C). We tested contractile function in attached collagen lattices with 10% serum for 4 days (with mitomycin C). Upon release, serum-treated 3T3 cells contract the lattice, but aR-KO cells fail to contract (Figure 5D). We treated cells with serum to examined MRTF nuclear accumulation, which revealed that nuclear MRTFA and MRTFB are diminished in aR-KO cells compared with wild type (WT) (Figure 5E). Interestingly, there is very little SRF in the nucleus of aR-KO cells regardless of treatment (Figure 5E). MRTF nuclear localization is governed by actin, such that G-actin binds to MRTF to keep it in the cytoplasm, and actin polymerization consumes G-actin to allow MRTF to accumulate in the nucleus (Guettler et al., 2008). But SRF is usually considered a nuclear protein, and unlike MRTF, SRF does not rapidly translocate in response to serum, nor does it interact with actin. To see if αSMA expression could be rescued, we generated aR-KO cells with a doxycycline-inducible MRTFA mutant that cannot bind actin, which renders it constitutively active, and found that this restores αSMA expression while also restoring SRF nuclear localization (Figure 5F). RhoGTPases promote SRF nuclear localization in airway smooth muscle cells (Liu et al., 2003), and PDGFRα can activate the RhoGTPase RAC1 (Feng et al., 2011; He and Soriano, 2013; Pickett et al., 2008). Consistent with this, serum fails to induce GTP-bound RAC1 in aR-KO cells (Figure 5G). To determine whether RAC1 is needed for SRF nuclear localization, we used small interfering RNA (siRNA) to knock down RAC1, which reduces SRF nuclear localization (Figure 5H). Therefore, PDGFRα is needed to activate RAC1 and localize SRF to the nucleus in 3T3 cells (Figure 5I).

To examine the fibroblast-to-myofibroblast transition in primary fibroblasts, we isolated DFs from *Pdgfra$^{Flp/+}$* and *Pdgfra$^{Flp/Flp}$* mice. However, both genotypes are similar in regard to αSMA expression, despite efficient deletion of PDGFRα (Figure S6E). Serum induces GTP-bound RAC1 in both genotypes, and SRF nuclear localization is not significantly different between genotypes (Figures S6F and S6G). However, RAC1 siRNA could block nuclear localization of SRF in *Pdgfra$^{Flp/+}$* DFs (Figure S6H). These results suggests that an unidentified factor upstream of RAC1 compensates for loss of PDGFRα in cultured primary

DFs. PDGFRβ can regulate SRF transcriptional activity in developing mural cells (Wang et al., 2004), and we noted that PDGFRβ is more highly expressed in primary DFs compared with 3T3 cells (Figure S6I, lanes 1–2 versus 3–4). Thus, it is conceivable for PDGFRβ to compensate for loss of PDGFRα in cultured primary DFs. However, the strong phenotype of *Ubc-Pdgfra^{Flp/Flp}* wounds indicates that it does not compensate *in vivo*. We conclude that loss of RAC1 and SRF activity in *Ubc-Pdgfra^{Flp/Flp}* progenitors may contribute to defective wound healing (Figure 5I).

Mrtfa/Mrtfb and Srf are both required for myofibroblast differentiation, but Srf alone is required for proliferation

Since MRTFs and PDGFRα appear to have different roles in Postn^+ myofibroblasts (Figures 3 and S4), we decided to test the role of MRTFs in PDGFRα^+ progenitors by generating *Pdgfra-Mrtfa^{−/−}b^{flox/flox}* mice with *Pdgfra^{CreER}*. Controls were mice without Cre or were *Mrtfa^{+/−}* (both denoted as *Mrtfab^{control}*) (Figures 6A–6C). Immunofluorescence confirms the deletion of MRTFB in *Pdgfra-Mrtfa^{−/−}b^{flox/flox}* wounds (Figure 6D). KO wounds at day 7 remain at their uncontracted width, and some fail to completely epithelialize (Figures 6E–6H). However, there is no difference in proliferation between KO and control wounds at day 4 (Figures 6I and 6J). Interestingly, KO wound beds are filled with *Pdgfra*-derived cells (Figure 6K) but are devoid of αSMA^+ myofibroblasts (Figures 6L–6O). The remaining αSMA^+ cells are mural cells, which are spared from *Mrtfb* deletion due to the specificity of *Pdgfra^{CreER}* to the fibroblast lineage. In summary, *Mrtfa/Mrtfb*-deficient wounds exhibit normal progenitor proliferation, and *Pdgfra*-derived cells can efficiently migrate into the wound bed, but myofibroblast differentiation is specifically abrogated. This is in contrast to *Pdgfra*-deficient wounds, which are deficient in progenitor proliferation and myofibroblast differentiation. This suggests that MRTFs and PDGFRα have different functions in the fibroblast-to-myofibroblast transition.

For comparison with *Mrtfa/Mrtfb*-deficient wounds, we generated *Pdgfra-Srf^{flox/flox}* mice and *Pdgfra-Srf^{flox/+}* controls (Figures 7A–7C). We confirmed that SRF protein is eliminated from *Pdgfra-Srf^{flox/flox}* wounds (Figure 7D). Like *Pdgfra*-deficient wounds, *Srf*-KO wounds display significant healing defects at day 7 (Figures 7E–7H). In day 4 wounds, we used a *Col1a1-GFP^{tg}* reporter to identify collagen-producing fibroblasts. EdU labeling of these cells is significantly reduced in KO wounds (Figures 7I and 7J). In *Srf*-KO wounds, the center of the wound bed lacks Tomato^+ *Pdgfra*-derived cells, and the few αSMA^+ myofibroblasts are restricted to the extreme edges of the wound (Figures 7K and 7L). The area of αSMA stain is significantly lower than in *Ubc-Pdgfra^{K/+}* wounds (Figure 1M), and myofibroblast differentiation of *Pdgfra*-derived cells is greatly reduced (Figures 7N and 7O). Overall, the healing defects resulting from *Srf* deletion in progenitors are similar to defects resulting from deletion of *Pdgfra* itself. This is consistent with SRF mediating the major functions of PDGFRα. In contrast, in *Mrtfa/Mrtfb*-deficient wounds, the specific loss of myofibroblasts without affecting progenitor proliferation/migration suggests distinct roles for PDGFRα and MRTF.

DISCUSSION

Understanding myofibroblast differentiation is critical for improving wound healing, reducing scarring, and unlocking regenerative potential. In this study, we used conditional mutations and lineage tracing to evaluate the transition of fibroblastic progenitors into myofibroblasts under different PDGF signaling conditions, in the absence of MRTFA and MRTFB, or in the absence of SRF (summarized in Figure S7 and Table S1). Although PDGF signaling is well known to promote fibrosis (Gallini et al., 2016; Klinkhammer et al., 2018; Olson and Soriano, 2009), and inhibition of PDGFRα in mice reduced fibrosis in organ-specific models (Abdollahi et al., 2005; Chen et al., 2014; Distler et al., 2007; Hayes et al., 2014; Horikawa et al., 2015; Makino et al., 2017; Mueller et al., 2016; Song et al., 2020), the specific role of PDGFRα in the fibroblast-to-myofibroblast transition has not been elucidated. Our results show that in early wound healing, progenitors require PDGFRα to support SRF activity and progenitor proliferation that is independent of MRTFs. This PDGFRα-SRF pathway should expand the progenitor population for later differentiation. Myofibroblast differentiation is then coordinated with downregulation of PDGFRα signaling, which may be necessary because our results suggest that PDGFRα opposes myofibroblast differentiation. Furthermore, because we observe fibrosis without myofibroblasts in PDGFRα^K mice with spontaneous fibrosis of the skin, muscle, heart, fat, and intestine (Figure S2), we conclude that PDGFRα is not sufficient to induce myofibroblast differentiation when acting alone.

We deleted or activated PDGFRα in periostin$^+$ myofibroblasts, but this did not lead to wound-healing defects, nor did it lead to activation of a reporter that depends on the intersection of *Posn*- and *Pdgfra*-driven recombinases. However, the same *Postn-MerCreMer* driver can generate wound-healing defects by deleting *Srf* (Davis et al., 2015) or by deleting *Mrtfb* on an *Mrtfa*$^{-/-}$ background (Figure S4), and it can directly activate a Cre-dependent Tomato reporter during wound healing. Therefore, our negative results with PDGFRα mutations argue that continual expression of PDGFRα is not required in myofibroblasts. This is in agreement with PDGFRα downregulation during normal wound healing and in mouse DFs treated with TGF-β1, which both occur in coordination with αSMA upregulation. TGF-β was previously shown to downregulate PDGFRα in fibro-adipogenic progenitors during muscle repair (Contreras et al., 2019). Contreras et al. highlighted TGF-β-p38 signaling as a pathway for downregulation of PDGFRα protein, but there are likely to be multiple mechanisms for PDGFRα protein and mRNA downregulation at the fibroblast-to-myofibroblast transition.

Conditional KO of *Pdgfra* before wounding results in impaired healing with reduced proliferation, ECM secretion, and myofibroblast differentiation. In this context, SRF appears to be more cytoplasmic. Further investigation with *Pdgfra* KO in 3T3 cells demonstrates that PDGFRα is indeed needed for SRF nuclear localization. In these *Pdgfra*-deficient cells, SRF mislocalization to the cytoplasm is correlated with depressed RAC1 activity. Further arguing for RAC1 having a role in SRF subcellular localization, knockdown of RAC1 in primary DFs shifted SRF to the cytoplasm. It remains to be tested whether RAC1 regulates SRF nuclear localization *in vivo*. However, conditional KO of *Rac1* in *Col1a2*-expressing cells led to wound-healing defects (Liu et al., 2009). SRF is regulated

by a variety of mechanisms including cofactor exchange (Gualdrini et al., 2016), mRNA stabilization (Davis et al., 2015), phosphorylation (Janknecht et al., 1992), and nuclear localization (Liu et al., 2003). Components of a PDGFRα-RAC1-SRF pathway have been previously suggested. In glioblastoma, activation of RAC1 by PDGFRα required the guanine nucleotide exchange factor Dock180 (Feng et al., 2011). In skeletal development, activation of RAC1 by PDGFRα required PI3K signaling (He and Soriano, 2013; Pickett et al., 2008). In craniofacial development, *Pdgfra* or *Srf* deletion in neural crest cells resulted in a cleft midface reminiscent of *Rac1* deletion in neural crest (Thomas et al., 2010; Vasudevan and Soriano, 2014). These findings provide evidence for a PDGFRα-RAC1-SRF pathway in diverse scenarios. However, although we find that 3T3 cells are dependent on PDGFRα and RAC1 for SRF nuclear localization, primary DFs require RAC1, but PDGFRα is not required. This suggests that cultured primary fibroblasts have PDGFRα-redundant pathways to activate RAC1 and SRF.

We find that defective SRF nuclear localization in *Pdgfra*-KO 3T3 cells is rescued by an MRTFA mutant that constitutively localizes to the nucleus. This rescue may result from nuclear MRTFA interacting with SRF to retain it in the nucleus, which does not imply that PDGFRα and MRTFs have a similar function in the fibroblast lineage. Indeed, KO of *Srf* with *Pdgfra-CreER* results in defective fibroblast proliferation and myofibroblast differentiation, which is similar to KO of *Pdgfra* itself (summarized in Figure S7). In contrast, deletion of *Mrtfa/Mrtfb* does not impair proliferation but profoundly blocks myofibroblast differentiation. These *in vivo* phenotypes argue that PDGFRα and MRTFs have distinct functions, both of which overlap with SRF functions.

Fibroblastic progenitors are still being identified in diverse organs (Plikus et al., 2021), with expression of PDGFRα typically required, but not sufficient, for their identity (Soliman et al., 2021). At rest, fibroblastic progenitors secrete organ-specific matrix and signaling proteins to maintain the organ stromal compartment. When activated in a wound, these cells proliferate, migrate, increase production of matrix proteins, and may transition into myofibroblasts or undergo differentiation into other cell types (e.g., adipocytes or osteoblasts), depending on the organ and extracellular cues. This study provides a rationale for temporal regulation of PDGFRα as a cell progresses through the fibroblast-to-myofibroblast transition. Negative cross-talk from PDGFRα to pro-myofibroblast signals like TGF-β may allow time for the proliferative phase of wound healing until TGF-β downregulates PDGFRα at an appropriate time for myofibroblast-driven scar maturation.

Limitations of the study

We investigated the function of genes in fibroblastic progenitors that differentiate into myofibroblasts. The precise origin of progenitors was not our focus. However, besides DFs, it has been shown that adipocytes and myeloid cells can also transition into myofibroblasts during wound healing (Guerrero-Juarez et al., 2019; Shook et al., 2020). In many organs, the adventitial layer of blood vessels has been identified as a niche for PDGFRα⁺ progenitors that give rise to myofibroblasts (Kramann et al., 2015; Sono et al., 2020). It is likely that all of these sources contribute progenitors, to differing degrees, to meet the demand for tissue repair in adult life. We note that in PDGFRα[K] mice, white adipose tissue displays

a perivascular pattern of fibrosis suggestive of adventitial progenitors (Figure S2E), as reported previously (Iwayama et al., 2015). We did not see this in the intestine or dermis or during skin wound healing. We did not monitor adipocyte regeneration from myofibroblasts because this process only occurs in larger wound sizes, not the 5 mm wounds we used here (Plikus et al., 2017). Finally, the mechanisms by which PDGFRα-RAC1 promotes SRF nuclear localization and how TGF-β downregulates PDGFRα are questions that remain to be investigated.

STAR★METHODS

RESOURCE AVAILABILITY

Lead contact—Further information and requests for resources and reagents should be directed to and will be fulfilled by the lead contact, Lorin E. Olson (lorin-olson@omrf.org).

Materials availability—All unique reagents generated in this study are available from the lead contact with a completed Materials Transfer Agreement.

Data and code availability—Numerical data reported in this paper will be shared by the lead contact upon request.

This paper does not report original code.

Any additional information required to reanalyze the data reported in this paper is available from the lead contact upon request.

EXPERIMENTAL MODEL AND SUBJECT DETAILS

Mice—See Table S1 for a summary of mouse strains used in this study. All animal experiments were performed according to procedures approved by the Institutional Animal Care and Use Committee at the Oklahoma Medical Research Foundation. Mice were maintained in a 12 hr light/dark cycle and housed in groups of two to five with unlimited access to water and food. All strains were maintained on a mixed C57BL/129 genetic background at room temperature. Both males and females were analyzed. All animal comparisons were age-matched and littermate controls were used whenever possible, except for *Ubc-Pdgfra$^{Flp/+}$* and *Ubc-Pdgfra$^{K/+}$* mice (Figure 1), which can only be generated by different breeding pairs. As a result, it is practical to perform experiments on *Ubc-Pdgfra$^{Flp/+}$*, *Ubc-Pdgfra$^{Flp/Flp}$*, and *Ubc-Pdgfra$^{K/+}$* mice at the same time, which is why the same F/+ control quantifications are used in Figures 1 and 4. The lines *Ubc-CreER^{tg}* (JAX:007001)(Ruzankina et al., 2007), *Pdgfra-Cre^{tg}* (JAX:013148)(Rivera-Gonzalez et al., 2016), *Postn^{MerCreMer}* (JAX:029645)(Kanisicak et al., 2016), *ROSA26^{Ai14}* (JAX:007914) (Madisen et al., 2010) and *Srf^{floxed}* (JAX:006658)(Miano et al., 2004) were purchased from the Jackson Laboratories. *Pdgfra$^{H2B:EGFP}$* (JAX:007669)(Hamilton et al., 2003) was from Philippe Soriano. The Flp/frt-regulated reporter *ROSA26$^{frt-STOP-frt-tdTomato}$* was modified from (JAX:021875)(Madisen et al., 2015) as described previously (Sun et al., 2020). *Pdgfra$^{flox-PDGFRa-flox-Flp}$* and *Pdgfra$^{flox-STOP-flox-PDGFRaK:Flp}$* were described previously (Sun et al., 2020). *Pdgfra^{CreER}* (JAX:032770)(Chung et al., 2018) was from Brigid Hogan

via Fabio Rossi. *Col1a1-GFP^tg* (Lin et al., 2008) was from David Brenner via Jeremy Duffield. *Mrtfa^null* and *Mrtfb^floxed* (Mokalled et al., 2010) was from Eric Olson.

Tamoxifen (Tmx) was prepared as a 20mg/mL stock in corn oil. To induce Cre recombination in 10-day-old mice, pups were gavaged once with 100 mg Tmx/kg bw. To induce Cre recombination before wounding, 6 – 9-week-old mice were gavaged three times with 100 mg Tmx/kg bw on alternating days, and wounds were created four days after the last treatment. To induce Cre recombination after wounding, wounded mice were gavaged with 100 mg Tmx/kg bw on days 1–3 after wounding. To create excisional wounds, mice were administered analgesic (Ketoprofen 5mg/kg) followed by inhaled anesthesia (5% isoflurane/1% oxygen). Dorsal hair was shaved and then completely removed using depilatory cream (Nair). The exposed skin was sterilized with 70% ethanol. Excisional wounding was performed using a 5mm biopsy punch to create 4 full-thickness dermal wounds. Mice were then single housed and wounds were left uncovered during healing. At the time of harvest (4 or 7-days post wounding), wound areas and a margin of unwounded skin were harvested and fixed in 4% paraformaldehyde overnight. For *in vivo* proliferation assays, mice were intraperitoneally injected with 200 μL of 2 mM EdU solution in 0.9% saline 4 hours before sacrifice.

Primary cells—Dermal fibroblasts were isolated from E18.5 fetuses (*Pdgfra^Flp/+* and *Pdgfra^Flp/Flp*) or 2 to 5-day-old pups (*Pdgfra^+/+* and *Pdgfra^K/+*) generated with *PdgfraCre^tg*. Skin was dissected and floated dermis-side down on 0.25% Trypsin at 37°C for 1 hour. Partially digested skin was then digested in DMEM + 500U/mL collagenase type II at 37°C for 1 hour with trituration every 15 minutes. After filtration through a 100 μm filter, cells were plated in growth medium consisting of DMEM/F12 supplemented with 10% Fetal Bovine Serum, L-glutamine, and 2mM penicillin/streptomycin and maintained at 37°C and 5% CO_2. Primary dermal fibroblasts were used for experiments at passage 2 or 3. Tomato expression was used to assess the rate of recombination. Cultures of *Pdgfra^Flp/+* and *Pdgfra^Flp/Flp* DF were 85–90% Tomato+ and *Pdgfra^K/+* cultures were >95% Tomato+. Primary fibroblasts were grown in DMEM/F12 supplemented with 10% Fetal Bovine Serum (FBS), L-glutamine, and 2mM penicillin/streptomycin and maintained at 37°C and 5% CO_2. For serum starvation, cells were grown in 0.1% FBS for 24 hours.

Cell lines—CRISPR/Cas9 was used to generate Pdgfra-knockout NIH/3T3 cell lines. First, Cas9-expressing cells were created by lentiviral transduction. To construct the vector, eCas9 1.1 was excised with Age1 and EcoR1 and ligated into pENTR eGFP C1X (gift from Dr. Eric Campeau) plasmid cut with the same restriction enzymes creating pENTR eCas9 1.1. Then pENTR eCas9 1.1 was mixed with pLenti CMV Hygro DEST and Clonase II to create the lentiviral expression construct pLenti CMV eCas9 1.1 Hygro, which was confirmed by sequencing. This lentiviral construct was used to generate VSV-G pseudotyped lentivirus as previously described (Berry et al., 2014). eCas9 1.1-expressing cells were selected with 100 μg/mL of hygromycin. Second, lentivirus expressing Pdgfra sgRNA was created by cloning the sgRNA (sequence: TGAGGACCAGAAAGACCTGG) into lenti-Guide Puro to create lenti-mm sgPDGFRα #2 Puro. This lentiviral construct was used to make VSV-G pseudotyped lentivirus. Lentivirus was incubated with NIH 3T3 eCas9

1.1 cells and subsequently selected with Puromycin. Cells resistant to Hygromycin and Puromycin were seeded as individual cells in a 96-well plate and allowed to expand to create *Pdgfra*-knockout (aR-KO) clonal cell lines. Individual clones were analyzed by Western blot to detect loss of protein. In addition, genomic DNA was PCR amplified from the clones denoted as NIH/3T3 aR-KO#2 and #3 using primers flanking the sgRNA targeting sequence found in the first coding exon (PdgfraEx1F and PdgfraEx1R, see Table S2). PCR product was subcloned and sequenced. Sequencing clone #2 showed a 5 base pair deletion (CAC CA) resulting in a frame-shift mutation creating a premature stop codon (5′-ATG GGG ACC TCC deletion GGT CTT TCT GGT CCT CAG CTG TCT CCT CAC AGG GCC GGG CCT CAT CTC CTG CCA GCT CTT ATT ACC CTC TAT CCT CCC AAA CGA GAA TGA-3′). Sequencing clone #3 showed deletion of the first coding exon. All NIH/3T3 cells were grown in DMEM supplemented with 10% FBS, L-glutamine, and 2mM penicillin/streptomycin and maintained at 37°C and 5% CO$_2$. For serum starvation, cells were grown in 0.1% FBS for 24 hours. *Doxycycline-inducible constitutively active (CA) MRTFA was introduced to aR-KO cells by lentivirus*. First, we amplified the mouse MRTFA cDNA (CloneID BC050941) with primers MRTFA- N-forward and MRTFA-reverse (Table S2), which generates a truncated MRTFA lacking the N-terminal RPEL domains that bind G-actin (Guettler et al., 2008). The amplicion was digested with Mfe1 and Sal1, then ligated into pENTR IRES iRFP720 digested with EcoR1 and Sal1. This clone was then recombined into pInducer 20 using Clonase II. After lentiviral transduction, aR-KO cells with CA-MRTFA were selected with 1mg/mL G418. Finally, aR-KO cells with CA-MRTFA were treated with 500ng/mL doxycycline for 48 hours to induce mutant MRTFA.

METHOD DETAILS

Histology and immunostaining of tissue—All tissues were fixed in 4% paraformaldehyde overnight at 4°C. For *histological stains*, paraffin sections were deparaffinized in Histoclear and then rehydrated through stepwise decreasing ethanol concentration to distilled water. For hematoxylin and eosin staining, slides were stained with Hematoxylin for 1 minute and then washed with tap water. Slides were then incubated in Eosin Y for 2–3 minutes and then washed again with tap water. The Picrosirius Red Stain (PSR) Kit was used for PSR staining and stained sections were imaged under polarized light. For *immunohistochemistry*, deparaffinized slides were incubated in 3% H$_2$O$_2$ diluted in methanol for 10 minutes to quench endogenous alkaline phosphatase activity and then washed in PBS 3 times. For antigen retrieval, slides were incubated for 15 minutes in steaming 10 mM sodium citrate buffer pH6.0 and then cooled to room temperature. Slides were blocked with 5% goat serum in PBS for 1 hour at room temperature prior to addition of primary antibody in PBS with 5% goat serum overnight at 4°C. PBS with 5% goat serum was used for no primary antibody negative controls. Slides were washed 3 times with PBS and then incubated with biotinylated goat anti-rabbit secondary antibody (Vectastain ABC Kit) in PBS with 5% goat serum for 1 hour at 4°C. Slides were washed 3 times in PBS and then incubated with the ABC complex (Vectastain ABC Kit) at room temperature for 1 hour. Following another 3 PBS washes, slides were developed (DAB Peroxidase Substrate Kit) and counterstained with hematoxylin. Slides were rinsed in tap water, dehydrated, mounted with Permount, dried, and imaged on a Nikon Eclipse 80i microscope. For *immunofluorescence*, deparaffinized slides or frozen slides were blocked with 5% donkey

serum in PBS for 1 hour, then incubated with primary antibody overnight a 4°C in a humidified chamber, then washed three times, then incubated with fluorescent secondary antibody for 1 hour. For EdU detection, slides with frozen or paraffin tissue sections were incubated with EdU reaction cocktail (175 μL PBS, 4 μL CuSO4, 0.2 μL Alexa Fluor 488 Azide, and 20 μL 0.5 M ascorbic acid) for 30 minutes in the dark at room temperature. Paraffin sections were subsequently stained with anti-RFP antibody for Tomato co-labeling. Frozen sections were not stained with anti-RFP because Tomato fluorescence was sufficient. After staining, slides were washed three times with PBS including one wash including DAPI, then coverslipped using Fluoro Gel with DABCO. After drying they were imaged on a Nikon Eclipse 80i microscope or Nikon C2+ confocal microscope. Due to the large size of many mutant wounds, imaging of entire wound beds typically required multiple individual microscope images to be assembled into one image.

Western blotting

__Whole cell extracts:__ Protein was extracted from cells with ice cold lysis buffer (50 mM Tris pH7.4, 150 mM NaCl, 1% NP-40, 0.1% SDS, 0.25% sodium deoxycholate) with the addition of protease and phosphatase inhibitors (Complete protease inhibitor cocktail, 1 mM EDTA, 1mM sodium orthovanadate, 1 mM NaF, 1mM PMSF). After 10 minutes incubation on ice, lysates were sonicated for 30 seconds, followed by incubation on ice for 30 minutes. The lysates were cleared by centrifugation.

__Nuclear and cytoplasmic extracts:__ cytoplasmic proteins were extracted by resuspending cells in ice cold hypotonic buffer (20 mM Tris pH7.4, 10 mM NaCl, 3 mM $MgCl_2$) with protease and phosphatase inhibitors followed by resting on ice for 20 min to allow cell swelling. Then 1/20 volume of 10% NP-40 was added to each suspension, which was then vortexted to disrupt cytoplasmic membranes. Nuclei were pelleted by centrifugation at 5000 rpm for 10 minutes and supernatant containing cytoplasmic extract was removed. Nuclei were then washed with a large volume of hypotonic buffer. Then clean nuclei were lysed in ice cold nuclear extract buffer (10 mM Tris pH7.4, 100 mM NaCl, 1% Triton X-100, 0.1% SDS, 0.5% sodium deoxycholate, 10% glycerol, 1 mM EDTA) with protease and phosphatase inhibitors. After 10 minutes incubation on ice, lysates were sonicated for 30 seconds, followed by incubation on ice for 30 minutes. The lysate was cleared by centrifugation. *For all extracts*, protein concentration was determined by BCA assay. Then denaturing loading buffer was added to each lysate, each was boiled for 10 minutes, and aliquots containing 5 μg of protein were separated by 8% or 12% gel SDS-PAGE, using parallel gels for proteins of similar size. In the case of nuclear and cytoplasmic extracts, 5 μg of each fraction was loaded on the same gel. As the cytoplasm accounts for ~75% of the total cellular protein, yet 5 μg of each fraction was loaded, the nuclear fractions will be over-represented in these blots relative to the cytoplasm. Proteins were transferred from gel to nitrocellulose membranes, blocked with 5% BSA, and then subjected to detection with primary antibodies in 5% BSA block. Membranes were then probed with horseradish-peroxidase conjugated antibodies diluted in 5% milk block. Primary and secondary antibodies were used at 1:1000–1:2000 and 1:5000, respectively. Blots were developed with ECL Western blotting substrate and autoradiography film.

RAC1-GTP detection—To detect the active, GTP-bound form of RAC1, we used Active RAC1 Detection Kit following the manufacturer's protocol. Cells were grown to 50% confluence, then serum starved for 24 hours, then treated with medium containing 10% FBS for 10 minutes. After lysis (buffer from the kit) and determination of protein concentration, input fractions were removed and stored. Then 500 μg protein of each lysate was interacted with recombinant GST-PAK1-PBD (from the kit), separated based on affinity for glutathione (resin from the kit). Bound protein was eluted from the resin with denaturing loading buffer and was separated by 12% gel SDS-PAGE. 5 μg of each input fraction was separated on the same gel as the bound protein. After transfer to nitrocellulose membranes, eluted RAC1 (RAC1-GTP) and input RAC1 (total RAC1) were detected by Western blotting with anti-RAC-1 antibody.

siRNA transfection—To knockdown RAC1, we used Lipofectamine RNAiMAX to introduce *Rac1* siRNA or control siRNA. Cells were grown to 50–70% confluence in 6 cm plates, then 3 μL of each siRNA was transfected according to manufacturer's instructions. After 48 hours, cells were harvested for nuclear and cytoplasmic extracts to be used for Western blotting.

Immunocytochemistry—Cells seeded on chamber slides were allowed to attach overnight, then fixed with 4% paraformaldehyde for 10 minutes. Cells were then permeabilized with 0.1% Triton-X100 and blocked in PBS with 5% donkey serum for 30 minutes. Then anti-αSMA antibody was applied at 1:250 with 5% donkey serum overnight at 4°C in a humidified chamber, then washed three times, then incubated with fluorescent secondary antibody at 1:250 and phalloidin at 1:100 for 1 hour, then washed three times with one wash including DAPI, then coverslipped using Fluoro Gel. After drying they were imaged on a Nikon Eclipse 80i microscope.

Collagen matrix contraction assays—Cells were cultured in three-dimensional type 1 collagen matrixes (collagen concentration, 1mg/ML; cell concentration, 1×10^6 cells/mL). Matrixes were formed from 0.25 mL of cell/collagen solution that was placed on a pre-warmed 35 mm TPP cell culture dish and allowed to polymerize for 5 minutes. Fibroblasts in matrixes were then cultured in complete medium with 10% FBS for 24 hours, followed by 4 days with 0.1% FBS or 10% FBS or 2ng/mL TGFβ−1. Mitomycin C (0.625 μg/mL) was add to the medium to suppress proliferation differences between control and mutant cells. Medium was replaced every 48 hours. After 5 days in culture, the matrixes were photographed, then gently detached from the bottom of the dish to allow contraction for 24 hours, then photographed again with a digital camera. Each experiment was repeated twice with similar results.

RNA isolation and quantitative RT-PCR (qPCR)—Total RNA was isolated from cultured cells or wound tissue using Trizol. cDNA reverse transcription was performed using random primers and SuperScript III RT. Quantitative PCR was performed on a CFX96 real-time PCR system (Bio-Rad) with iQ SYBR Green master mix (Bio-Rad). Bio-Rad CFX Manager (V2.1) software was used for analyzing cycle threshold (Ct) values and melting

curves. Fold differences in mRNA levels were normalized to the expression of *Gapdh*. Primer sequences are listed in Table S2.

Genomic DNA isolation and genotyping Cre-recombination by PCR—To verify Cre-recombination of the $Pdgfra^{Flp}$ and $Pdgfra^{K}$ alleles when combined with $Postn^{MCM}$, genomic DNA was isolated from unwounded skin or wound tissue by digesting with proteinase K followed by phenol/chloroform extraction. Then 35 cycles of PCR were performed with 200 ng of DNA. To detect the Cre-recombination product of the lox-PDGFRα:STOP-lox-Flp° cassette in $Pdgfra^{Flp}$ mice, SA-Forward and Flpo-Reverse primers were used. To detect the Cre-recombination product of the lox-STOP-lox-PDGFRαK-T2A-Flp° cassette in $Pdgfra^{K}$ mice, SA-Forward and aK-Reverse primers were used. Positive control DNA was isolated from $Pdgfra^{Flp}$ and $Pdgfra^{K}$ mice with *Sox2Cre*. Primer sequences are listed in Table S2.

QUANTIFICATION AND STATISTICAL ANALYSIS

Statistical analysis—Data are presented as means +/− SEM or +/− SD as indicated in the figure legends. Differences were analyzed by unpaired two-tailed Student's t test between two groups using Graphpad Prism 9. All measurements were from distinct biological samples (individual mice). Statistical parameters are found in the figure legends, including exact n and number of biological repeats. Each mouse was considered a biological replicate.

Quantification of wound bed area, wound contraction, and % epithelialization—Day 7 wounds were embedded in paraffin and sectioned through the center of the wound. Tissue sections were stained with hematoxylin and eosin. Digital microscope images were captured. Quantification was performed using ImageJ. Wound bed area was defined as the area bounded by the intact dermis flanking each side of the wound, the scab or new epidermis above, and the fascia or bottom of the tissue sample below. To calculate wound contraction, the wound width from intact dermis to intact dermis was measured and divided by the original wound width (5 mm). To calculate epithelialization, the two epithelial tongues were measured and their combined length was divided by the wound width.

Quantification of αSMA⁺ area and intensity of PDGFRα in wound tissue—Day 5 or day 7 wounds from wild type mice were cryosectioned through the center of the wound. Tissue sections were stained with antibody to detect αSMA or PDGFRα, followed by anti-rabbit or anti-goat secondary antibody with fluorescent conjugate. Digital microscope images were captured. Quantification of αSMA⁺ area and wound bed area were performed using ImageJ, then converted to a percentage. Quantification of PDGFRα staining intensity was performed using ImageJ to measure wound bed area, total PDGFRα fluorescence, and background fluorescence. After normalizing for area, the background fluorescence was subtracted from the total PDGFRα fluorescence to determine corrected fluorescence integrated density expressed as relative fluorescence units (RFU).

Quantification of cell proliferation and myofibroblast differentiation—For proliferation measurements, day 4 wounds were cryosectioned through the center of the wound. Tissue sections were stained for EdU and digital microscope images were captured

with EdU, Tomato, and DAPI. Between 100 and 350 Tomato$^+$ cells were scored per mouse, except for Figure 7 where Col1a1-EGFP$^+$ cells were counted. For each mouse the % EdU$^+$ cells among the fluorescent population, or the proliferation index, was calculated by dividing the number of EdU$^+$Tomato/EGFP$^+$ cells counted by the total number of Tomato/EGFP$^+$ cells counted. For myofibroblast measurements, day 7 wounds were cryosectioned through the center of the wound. Tissue sections were stained for αSMA and confocal microscope images were captured with αSMA, Tomato, and DAPI. Between 100 and 1600 Tomato$^+$ cells were scored per mouse. For each mouse the % αSMA$^+$ cells among the Tomato$^+$ population, or the myofibroblast index, was calculated by dividing the number of αSMA$^+$Tomato$^+$ cells counted by the total number of Tomato$^+$ cells counted. Quantification was performed manually. Experiments were not blinded, as the mouse genotypes were known prior to analysis. In some cases, blinding was impossible because wound morphology or labeling patterns revealed the genotype.

Quantification of collagen matrix contraction—The diameter of each matrix before contraction and at various time intervals after release was measured using digital images and Image J software. The percent of initial lattice area was calculated by dividing the final matrix area (24 hour time point) by the area before contraction. Contraction assays were performed three times with different biological replicates of each genotype.

Supplementary Material

Refer to Web version on PubMed Central for supplementary material.

ACKNOWLEDGMENTS

REFERENCES

Abdollahi A, Li M, Ping G, Plathow C, Domhan S, Kiessling F, Lee LB, McMahon G, Gröne HJ, Lipson KE, et al. (2005). Inhibition of platelet-derived growth factor signaling attenuates pulmonary fibrosis. J. Exp. Med. 201, 925–935. [PubMed: 15781583]

Andrae J, Gallini R, and Betsholtz C (2008). Role of platelet-derived growth factors in physiology and medicine. Genes Dev. 22, 1276–1312. [PubMed: 18483217]

Beer HD, Longaker MT, and Werner S (1997). Reduced expression of PDGF and PDGF receptors during impaired wound healing. J. Invest. Dermatol. 109, 132–138. [PubMed: 9242497]

Berry WL, Kim TD, and Janknecht R (2014). Stimulation of beta-catenin and colon cancer cell growth by the KDM4B histone demethylase. Int. J. Oncol. 44, 1341–1348. [PubMed: 24481461]

Bugg D, Bailey LRJ, Bretherton RC, Beach KE, Reichardt IM, Robeson KZ, Reese AC, Gunaje J, Flint G, DeForest CA, et al. (2022). MBNL1 drives dynamic transitions between fibroblasts and myofibroblasts in cardiac wound healing. Cell Stem Cell 29, 419–433.e10. [PubMed: 35176223]

Campeau E, Ruhl VE, Rodier F, Smith CL, Rahmberg BL, Fuss JO, Campisi J, Yaswen P, Cooper PK, and Kaufman PD (2009). A versatile viral system for expression and depletion of proteins in mammalian cells. PLoS One 4, e6529. [PubMed: 19657394]

Chen YT, Chang YT, Pan SY, Chou YH, Chang FC, Yeh PY, Liu YH, Chiang WC, Chen YM, Wu KD, et al. (2014). Lineage tracing reveals distinctive fates for mesothelial cells and submesothelial fibroblasts during peritoneal injury. J. Am. Soc. Nephrol. 25, 2847–2858. [PubMed: 24854266]

Chung MI, Bujnis M, Barkauskas CE, Kobayashi Y, and Hogan BLM (2018). Niche-mediated BMP/SMAD signaling regulates lung alveolar stem cell proliferation and differentiation. Development 145, dev163014. [PubMed: 29752282]

Contreras O, Cruz-Soca M, Theret M, Soliman H, Tung LW, Groppa E, Rossi FM, and Brandan E (2019). Cross-talk between TGF-beta and PDGFRalpha signaling pathways regulates the fate of stromal fibro-adipogenic progenitors. J. Cell Sci. 132, jcs232157. [PubMed: 31434718]

Crider BJ, Risinger GM Jr., Haaksma CJ, Howard EW, and Tomasek JJ (2011). Myocardin-related transcription factors A and B are key regulators of TGF-beta1-induced fibroblast to myofibroblast differentiation. J. Invest. Dermatol. 131, 2378–2385. [PubMed: 21776010]

Davis J, Salomonis N, Ghearing N, Lin SCJ, Kwong JQ, Mohan A, Swanson MS, and Molkentin JD (2015). MBNL1-mediated regulation of differentiation RNAs promotes myofibroblast transformation and the fibrotic response. Nat. Commun. 6, 10084. [PubMed: 26670661]

Dinsmore CJ, and Soriano P (2022). Differential regulation of cranial and cardiac neural crest by serum response factor and its cofactors. Elife 11, e75106. [PubMed: 35044299]

Distler JHW, Jüngel A, Huber LC, Schulze-Horsel U, Zwerina J, Gay RE, Michel BA, Hauser T, Schett G, Gay S, et al. (2007). Imatinib mesylate reduces production of extracellular matrix and prevents development of experimental dermal fibrosis. Arthritis Rheum. 56, 311–322. [PubMed: 17195235]

Driskell RR, Lichtenberger BM, Hoste E, Kretzschmar K, Simons BD, Charalambous M, Ferron SR, Herault Y, Pavlovic G, Ferguson-Smith AC, et al. (2013). Distinct fibroblast lineages determine dermal architecture in skin development and repair. Nature 504, 277–281. [PubMed: 24336287]

Esnault C, Stewart A, Gualdrini F, East P, Horswell S, Matthews N, and Treisman R (2014). Rho-actin signaling to the MRTF coactivators dominates the immediate transcriptional response to serum in fibroblasts. Genes Dev. 28, 943–958. [PubMed: 24732378]

Feng H, Hu B, Liu KW, Li Y, Lu X, Cheng T, Yiin JJ, Lu S, Keezer S, Fenton T, et al. (2011). Activation of Rac1 by Src-dependent phosphorylation of Dock180(Y1811) mediates PDGFRalpha-stimulated glioma tumorigenesis in mice and humans. J. Clin. Invest. 121, 4670–4684. [PubMed: 22080864]

Gallini R, Lindblom P, Bondjers C, Betsholtz C, and Andrae J (2016). PDGF-A and PDGF-B induces cardiac fibrosis in transgenic mice. Exp. Cell Res. 349, 282–290. [PubMed: 27816607]

Greenhalgh DG, Sprugel KH, Murray MJ, and Ross R (1990). PDGF and FGF stimulate wound healing in the genetically diabetic mouse. Am. J. Pathol. 136, 1235–1246. [PubMed: 2356856]

Gualdrini F, Esnault C, Horswell S, Stewart A, Matthews N, and Treisman R (2016). SRF Cofactors control the balance between cell proliferation and contractility. Mol. Cell 64, 1048–1061. [PubMed: 27867007]

Guerrero-Juarez CF, Dedhia PH, Jin S, Ruiz-Vega R, Ma D, Liu Y, Yamaga K, Shestova O, Gay DL, Yang Z, et al. (2019). Single-cell analysis reveals fibroblast heterogeneity and myeloid-derived adipocyte progenitors in murine skin wounds. Nat. Commun. 10, 650. [PubMed: 30737373]

Guettler S, Vartiainen MK, Miralles F, Larijani B, and Treisman R (2008). RPEL motifs link the serum response factor cofactor MAL but not myocardin to Rho signaling via actin binding. Mol. Cell Biol. 28, 732–742. [PubMed: 18025109]

Gurtner GC, Werner S, Barrandon Y, and Longaker MT (2008). Wound repair and regeneration. Nature 453, 314–321. [PubMed: 18480812]

Hamilton TG, Klinghoffer RA, Corrin PD, and Soriano P (2003). Evolutionary divergence of platelet-derived growth factor alpha receptor signaling mechanisms. Mol. Cell Biol. 23, 4013–4025. [PubMed: 12748302]

Hayes BJ, Riehle KJ, Shimizu-Albergine M, Bauer RL, Hudkins KL, Johansson F, Yeh MM, Mahoney WM Jr., Yeung RS, and Campbell JS (2014). Activation of platelet-derived growth factor receptor alpha contributes to liver fibrosis. PLoS One 9, e92925. [PubMed: 24667490]

He F, and Soriano P (2013). A critical role for PDGFRalpha signaling in medial nasal process development. PLoS Genet. 9, e1003851. [PubMed: 24086166]

Heldin CH, and Westermark B (1999). Mechanism of action and in vivo role of platelet-derived growth factor. Physiol. Rev. 79, 1283–1316. [PubMed: 10508235]

Henderson NC, Rieder F, and Wynn TA (2020). Fibrosis: from mechanisms to medicines. Nature 587, 555–566. [PubMed: 33239795]

Hill CS, Wynne J, and Treisman R (1995). The Rho-family Gtpases Rhoa, Rac1, and Cdc42hs regulate transcriptional activation by Srf. Cell 81, 1159–1170. [PubMed: 7600583]

Hinz B (2007). Formation and function of the myofibroblast during tissue repair. J. Invest. Dermatol. 127, 526–537. [PubMed: 17299435]

Hoch RV, and Soriano P (2003). Roles of PDGF in animal development. Development 130, 4769–4784. [PubMed: 12952899]

Horikawa S, Ishii Y, Hamashima T, Yamamoto S, Mori H, Fujimori T, Shen J, Inoue R, Nishizono H, Itoh H, et al. (2015). PDGFRalpha plays a crucial role in connective tissue remodeling. Sci. Rep. 5, 17948. [PubMed: 26639755]

Iwayama T, Steele C, Yao L, Dozmorov MG, Karamichos D, Wren JD, and Olson LE (2015). PDGFRalpha signaling drives adipose tissue fibrosis by targeting progenitor cell plasticity. Genes Dev. 29, 1106–1119. [PubMed: 26019175]

Janknecht R, Hipskind RA, Houthaeve T, Nordheim A, and Stunnenberg HG (1992). Identification of multiple SRF N-terminal phosphorylation sites affecting DNA binding properties. EMBO J. 11, 1045–1054. [PubMed: 1547771]

Joe AWB, Yi L, Natarajan A, Le Grand F, So L, Wang J, Rudnicki MA, and Rossi FMV (2010). Muscle injury activates resident fibro/adipogenic progenitors that facilitate myogenesis. Nat. Cell Biol. 12, 153–163. [PubMed: 20081841]

Kanisicak O, Khalil H, Ivey MJ, Karch J, Maliken BD, Correll RN, Brody MJ, J Lin SC, Aronow BJ, Tallquist MD, et al. (2016). Genetic lineage tracing defines myofibroblast origin and function in the injured heart. Nat. Commun. 7, 12260. [PubMed: 27447449]

Klinkhammer BM, Floege J, and Boor P (2018). PDGF in organ fibrosis. Mol. Aspects Med. 62, 44–62. [PubMed: 29155002]

Kramann R, Schneider RK, DiRocco DP, Machado F, Fleig S, Bondzie PA, Henderson JM, Ebert BL, and Humphreys BD (2015). Perivascular gli1(+) progenitors are key contributors to injury-induced organ fibrosis. Cell Stem Cell 16, 51–66. [PubMed: 25465115]

Li R, Bernau K, Sandbo N, Gu J, Preissl S, and Sun X (2018). Pdgfra marks a cellular lineage with distinct contributions to myofibroblasts in lung maturation and injury response. Elife 7, e36865. [PubMed: 30178747]

Lin SL, Kisseleva T, Brenner DA, and Duffield JS (2008). Pericytes and perivascular fibroblasts are the primary source of collagen-producing cells in obstructive fibrosis of the kidney. Am. J. Pathol. 173, 1617–1627. [PubMed: 19008372]

Liu HW, Halayko AJ, Fernandes DJ, Harmon GS, McCauley JA, Kocieniewski P, McConville J, Fu Y, Forsythe SM, Kogut P, et al. (2003). The RhoA/Rho kinase pathway regulates nuclear localization of serum response factor. Am. J. Respir. Cell Mol. Biol. 29, 39–47. [PubMed: 12600823]

Liu S, Kapoor M, and Leask A (2009). Rac1 expression by fibroblasts is required for tissue repair in vivo. Am. J. Pathol. 174, 1847–1856. [PubMed: 19349358]

Madisen L, Garner AR, Shimaoka D, Chuong AS, Klapoetke NC, Li L, van der Bourg A, Niino Y, Egolf L, Monetti C, et al. (2015). Transgenic mice for intersectional targeting of neural sensors and effectors with high specificity and performance. Neuron 85, 942–958. [PubMed: 25741722]

Madisen L, Zwingman TA, Sunkin SM, Oh SW, Zariwala HA, Gu H, Ng LL, Palmiter RD, Hawrylycz MJ, Jones AR, et al. (2010). A robust and high-throughput Cre reporting and characterization system for the whole mouse brain. Nat. Neurosci. 13, 133–140. [PubMed: 20023653]

Makino K, Makino T, Stawski L, Mantero JC, Lafyatis R, Simms R, and Trojanowska M (2017). Blockade of PDGF receptors by crenolanib has therapeutic effect in patient fibroblasts and

in preclinical models of systemic sclerosis. J. Invest. Dermatol. 137, 1671–1681. [PubMed: 28433542]

Meerbrey KL, Hu G, Kessler JD, Roarty K, Li MZ, Fang JE, Herschkowitz JI, Burrows AE, Ciccia A, Sun T, et al. (2011). The pINDUCER lentiviral toolkit for inducible RNA interference in vitro and in vivo. Proc. Natl. Acad. Sci. USA 108, 3665–3670. [PubMed: 21307310]

Meyer-Ter-Vehn T, Gebhardt S, Sebald W, Buttmann M, Grehn F, Schlunck G, and Knaus P (2006). p38 inhibitors prevent TGF-beta-induced myofibroblast transdifferentiation in human tenon fibroblasts. Invest. Ophthalmol. Vis. Sci. 47, 1500–1509. [PubMed: 16565385]

Miano JM (2003). Serum response factor: toggling between disparate programs of gene expression. J. Mol. Cell. Cardiol. 35, 577–593. [PubMed: 12788374]

Miano JM, Ramanan N, Georger MA, de Mesy Bentley KL, Emerson RL, Balza RO Jr., Xiao Q, Weiler H, Ginty DD, and Misra RP (2004). Restricted inactivation of serum response factor to the cardiovascular system. Proc. Natl. Acad. Sci. USA 101, 17132–17137. [PubMed: 15569937]

Mokalled MH, Johnson A, Kim Y, Oh J, and Olson EN (2010). Myocardin-related transcription factors regulate the Cdk5/Pctaire1 kinase cascade to control neurite outgrowth, neuronal migration and brain development. Development 137, 2365–2374. [PubMed: 20534669]

Mueller AA, van Velthoven CT, Fukumoto KD, Cheung TH, and Rando TA (2016). Intronic polyadenylation of PDGFRalpha in resident stem cells attenuates muscle fibrosis. Nature 540, 276–279. [PubMed: 27894125]

Muhl L, Genové G, Leptidis S, Liu J, He L, Mocci G, Sun Y, Gustafsson S, Buyandelger B, Chivukula IV, et al. (2020). Single-cell analysis uncovers fibroblast heterogeneity and criteria for fibroblast and mural cell identification and discrimination. Nat. Commun. 11, 3953. [PubMed: 32769974]

Olson LE, and Soriano P (2009). Increased PDGFRalpha activation disrupts connective tissue development and drives systemic fibrosis. Dev. Cell 16, 303–313. [PubMed: 19217431]

Pickett EA, Olsen GS, and Tallquist MD (2008). Disruption of PDGFRalpha-initiated PI3K activation and migration of somite derivatives leads to spina bifida. Development 135, 589–598. [PubMed: 18192285]

Pipes GCT, Creemers EE, and Olson EN (2006). The myocardin family of transcriptional coactivators: versatile regulators of cell growth, migration, and myogenesis. Genes Dev. 20, 1545–1556. [PubMed: 16778073]

Plikus MV, Guerrero-Juarez CF, Ito M, Li YR, Dedhia PH, Zheng Y, Shao M, Gay DL, Ramos R, Hsi TC, et al. (2017). Regeneration of fat cells from myofibroblasts during wound healing. Science 355, 748–752. [PubMed: 28059714]

Plikus MV, Wang X, Sinha S, Forte E, Thompson SM, Herzog EL, Driskell RR, Rosenthal N, Biernaskie J, and Horsley V (2021). Fibroblasts: origins, definitions, and functions in health and disease. Cell 184, 3852–3872. [PubMed: 34297930]

Rinkevich Y, Walmsley GG, Hu MS, Maan ZN, Newman AM, Drukker M, Januszyk M, Krampitz GW, Gurtner GC, Lorenz HP, et al. (2015). Skin fibrosis. Identification and isolation of a dermal lineage with intrinsic fibrogenic potential. Science 348, aaa2151. [PubMed: 25883361]

Rivera-Gonzalez GC, Shook BA, Andrae J, Holtrup B, Bollag K, Betsholtz C, Rodeheffer MS, and Horsley V (2016). Skin adipocyte stem cell self-renewal is regulated by a PDGFA/AKT-Signaling Axis. Cell Stem Cell 19, 738–751. [PubMed: 27746098]

Ruzankina Y, Pinzon-Guzman C, Asare A, Ong T, Pontano L, Cotsarelis G, Zediak VP, Velez M, Bhandoola A, and Brown EJ (2007). Deletion of the developmentally essential gene ATR in adult mice leads to age-related phenotypes and stem cell loss. Cell Stem Cell 1, 113–126. [PubMed: 18371340]

Sanjana NE, Shalem O, and Zhang F (2014). Improved vectors and genome-wide libraries for CRISPR screening. Nat. Methods 11, 783–784. [PubMed: 25075903]

Shook BA, Wasko RR, Mano O, Rutenberg-Schoenberg M, Rudolph MC, Zirak B, Rivera-Gonzalez GC, López-Giráldez F, Zarini S, Rezza A, et al. (2020). Dermal adipocyte lipolysis and myofibroblast conversion are required for efficient skin repair. Cell Stem Cell 26, 880–895.e6. [PubMed: 32302523]

Shook BA, Wasko RR, Rivera-Gonzalez GC, Salazar-Gatzimas E, López-Giráldez F, Dash BC, Muñoz-Rojas AR, Aultman KD, Zwick RK, Lei V, et al. (2018). Myofibroblast proliferation and

heterogeneity are supported by macrophages during skin repair. Science 362, eaar2971. [PubMed: 30467144]

Slaymaker IM, Gao L, Zetsche B, Scott DA, Yan WX, and Zhang F (2016). Rationally engineered Cas9 nucleases with improved specificity. Science 351, 84–88. [PubMed: 26628643]

Small EM, Thatcher JE, Sutherland LB, Kinoshita H, Gerard RD, Richardson JA, Dimaio JM, Sadek H, Kuwahara K, and Olson EN (2010). Myocardin-related transcription factor-a controls myofibroblast activation and fibrosis in response to myocardial infarction. Circ. Res. 107, 294–304. [PubMed: 20558820]

Soliman H, Theret M, Scott W, Hill L, Underhill TM, Hinz B, and Rossi FMV (2021). Multipotent stromal cells: one name, multiple identities. Cell Stem Cell 28, 1690–1707. [PubMed: 34624231]

Song K, Qing Y, Guo Q, Peden EK, Chen C, Mitch WE, Truong L, and Cheng J (2020). PDGFRA in vascular adventitial MSCs promotes neointima formation in arteriovenous fistula in chronic kidney disease. JCI Insight 5, 137298. [PubMed: 33001865]

Sono T, Hsu CY, Wang Y, Xu J, Cherief M, Marini S, Huber AK, Miller S, Péault B, Levi B, et al. (2020). Perivascular fibro-adipogenic progenitor tracing during post-traumatic osteoarthritis. Am. J. Pathol. 190, 1909–1920. [PubMed: 32533926]

Sun C, Berry WL, and Olson LE (2017). PDGFRalpha controls the balance of stromal and adipogenic cells during adipose tissue organogenesis. Development 144, 83–94. [PubMed: 28049691]

Sun C, Sakashita H, Kim J, Tang Z, Upchurch GM, Yao L, Berry WL, Griffin TM, and Olson LE (2020). Mosaic mutant analysis identifies PDGFRalpha/PDGFRbeta as negative regulators of adipogenesis. Cell Stem Cell 26, 707–721.e5. [PubMed: 32229310]

Thomas PS, Kim J, Nunez S, Glogauer M, and Kaartinen V (2010). Neural crest cell-specific deletion of Rac1 results in defective cell-matrix interactions and severe craniofacial and cardiovascular malformations. Dev. Biol. 340, 613–625. [PubMed: 20184871]

Todaro GJ, and Green H (1963). Quantitative studies of the growth of mouse embryo cells in culture and their development into established lines. J. Cell Biol. 17, 299–313. [PubMed: 13985244]

Tomasek JJ, Gabbiani G, Hinz B, Chaponnier C, and Brown RA (2002). Myofibroblasts and mechano-regulation of connective tissue remodelling. Nat. Rev. Mol. Cell Biol. 3, 349–363. [PubMed: 11988769]

Uezumi A, Ito T, Morikawa D, Shimizu N, Yoneda T, Segawa M, Yamaguchi M, Ogawa R, Matev MM, Miyagoe-Suzuki Y, et al. (2011). Fibrosis and adipogenesis originate from a common mesenchymal progenitor in skeletal muscle. J. Cell Sci. 124, 3654–3664. [PubMed: 22045730]

Vasudevan HN, and Soriano P (2014). SRF regulates craniofacial development through selective recruitment of MRTF cofactors by PDGF signaling. Dev. Cell 31, 332–344. [PubMed: 25453829]

Velasquez LS, Sutherland LB, Liu Z, Grinnell F, Kamm KE, Schneider JW, Olson EN, and Small EM (2013). Activation of MRTF-A-dependent gene expression with a small molecule promotes myofibroblast differentiation and wound healing. Proc. Natl. Acad. Sci. USA 110, 16850–16855. [PubMed: 24082095]

Wang Z, Wang DZ, Hockemeyer D, McAnally J, Nordheim A, and Olson EN (2004). Myocardin and ternary complex factors compete for SRF to control smooth muscle gene expression. Nature 428, 185–189. [PubMed: 15014501]

Werner S, and Grose R (2003). Regulation of wound healing by growth factors and cytokines. Physiol. Rev. 83, 835–870. [PubMed: 12843410]

Highlights

- Elevated PDGFRα signaling delays myofibroblast differentiation in wound healing

- PDGFRα deletion reduces proliferation and myofibroblast differentiation

- Early wound healing involves overlapping functions of SRF and PDGFRα

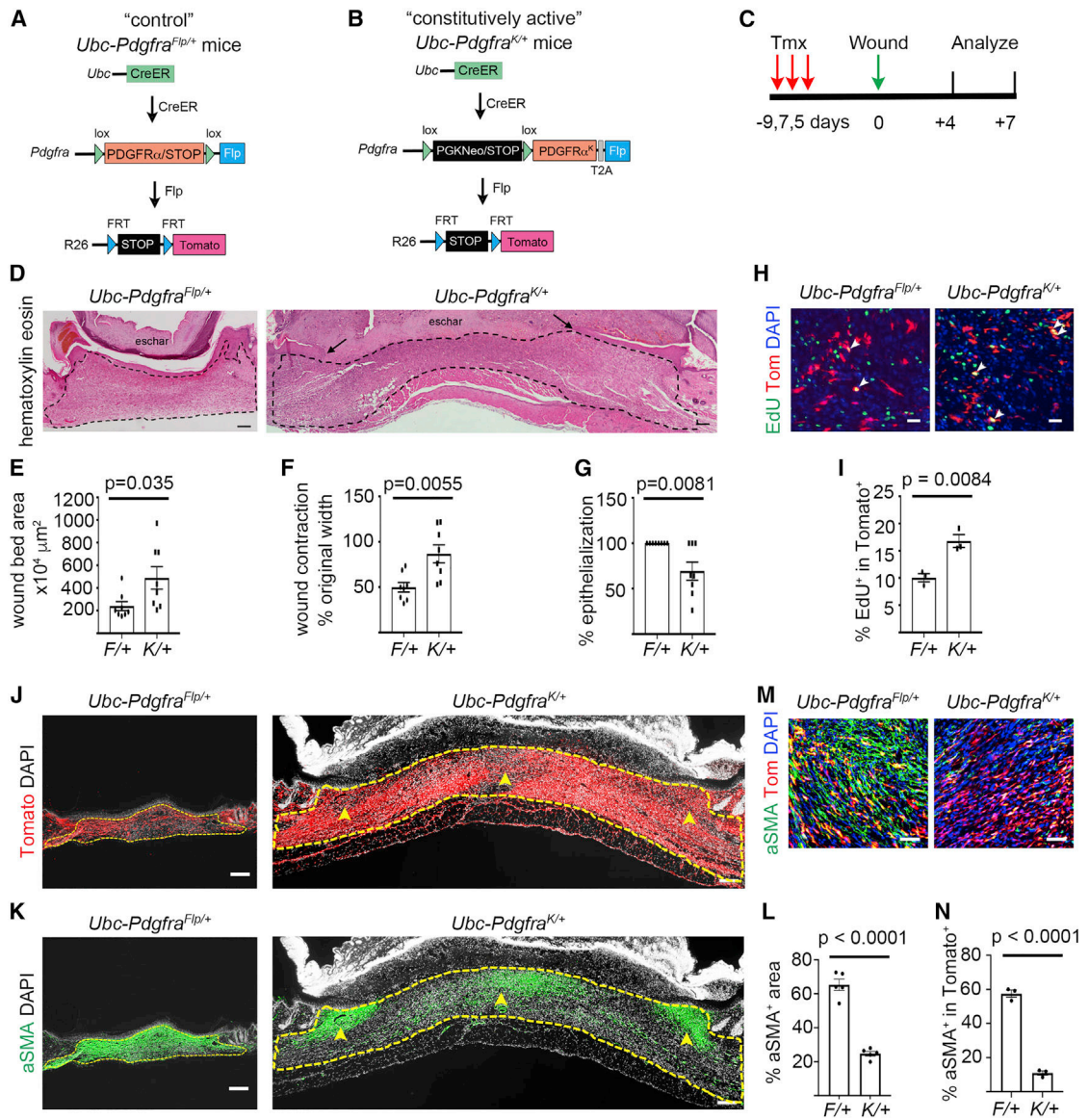- MRTF and PDGFRα have distinct functions in early versus late wound healing

Figure 1. PDGFRα^K delays myofibroblast differentiation in wound healing

(A–C) Schematic of the genetic labeling strategy for *Ubc-Pdgfra^{Flp/+}* control mice (A) and *Ubc-Pdgfra^{K/+}* constitutively active mice (B) and the timeline (C).

(D–G) Histology and histomorphometry at the wound center on day 7 (n = 8 of each genotype). H&E staining: the mutant wound is filled with granulation tissue but remains uncontracted with widely separated epithelial tongues (arrows). Dotted lines indicate the wound bed area (D). Wound bed cross-sectional area (E). Wound contraction as a percentage of the original 5 mm width (F). Percentage of wound width covered with epithelium (G). Scale bars, 200 μm.

(H and I) EdU/Tomato co-labeling of proliferating cells on day 4. Arrowheads indicate EdU⁺Tomato⁺ cells (H). Quantification of EdU in Tomato⁺ cells (n = 3 mice per genotype) (I). Scale bars 50 μm.

(J and K) Tomato and αSMA at the wound center on day 7. Arrowheads indicate regions of low Tomato. Dotted lines indicate the wound bed area. Scale bars, 200 μm.

(L) Quantification of αSMA$^+$ area on day 7 (n = 5 mice per genotype).

(M and N) αSMA/Tomato co-labeling on day 7 (M). Quantification of αSMA in Tomato$^+$ cells (n = 3 mice per genotype) (N). Scale bar, 50 μm. Data are plotted as mean ± SEM. Each point represents one mouse.

Note: experiments in Figures 1 and 4 were performed at the same time, so the *Fl*/+ control quantifications are the same between the two figures.
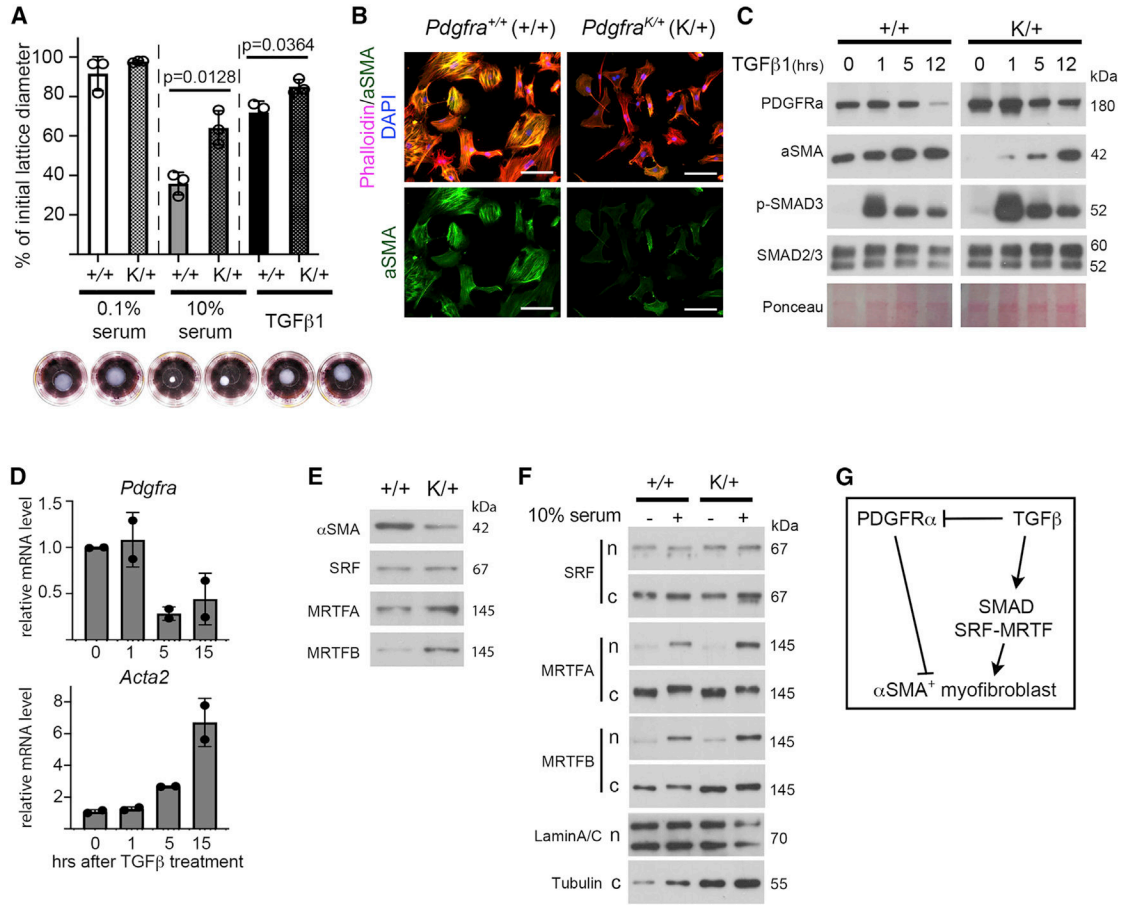
See also Figures S1 and S2.

Figure 2. PDGFRα^K opposes myofibroblast differentiation and is opposed by TGF-β.

(A–F) Primary dermal fibroblasts (DFs) assayed at passage 2–3.

(A) Collagen lattice contraction, expressed as a percentage of the initial diameter, with representative images at 24 h after lattice detachment (n = 3 biological replicates per genotype). Data are plotted as mean ± SD. Each point represents one biological replicate.

(B) DF stained for F-actin and αSMA. Scale bar, 50 μm.

(C) DF serum starved and treated with 10 ng/mL TGF-β1, then processed for western blot. TGF-β1 downregulates PDGFRα while upregulating αSMA with SMAD3 phosphorylation. Effects of TGF-β1 are delayed in *Pdgfra^K/+* DFs.

(D) qPCR for *Pdgfra* or *Acta2* in DFs treated with TGF-β1 as above (n = 2 biological replicates).

(E) Western blot for αSMA, SRF, MRTFA, and MRTFB in serum-starved DFs.

(F) Western blot with nuclear (n) and cytoplasmic (c) fractions after serum starvation followed by serum for 30 min

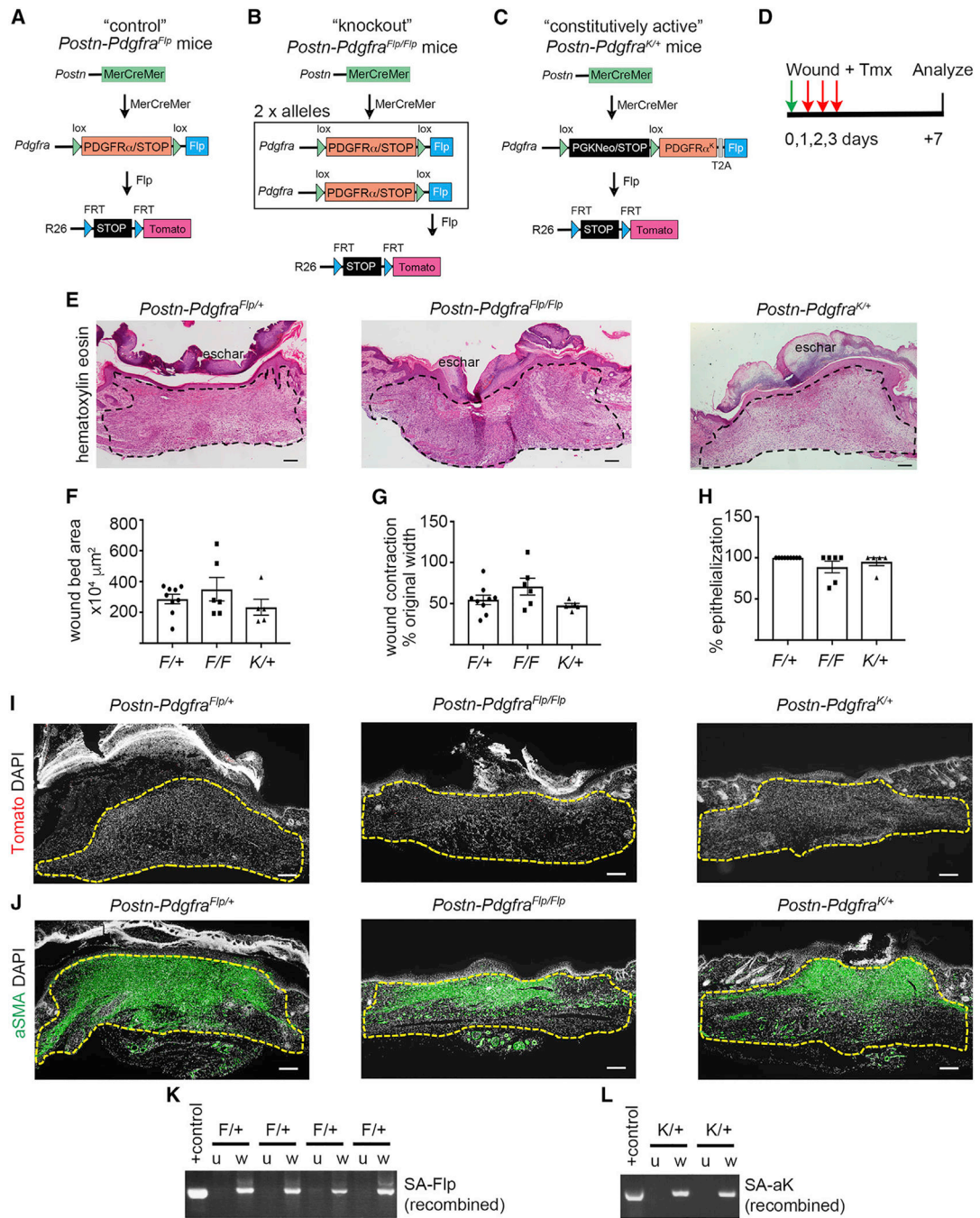(G) Summary of the proposed PDGFRα-TGF-β-myofibroblast relationship.

Figure 3. Pdgfra is not required in Postn$^+$ myofibroblasts

(A–D) Schematic of the genetic labeling strategy for *Postn-Pdgfra$^{F/+}$* control mice (A), *Postn-Pdgfra$^{F/F}$* knockout mice (B), and *Postn-Pdgfra$^{K/+}$* constitutively active mice (C) and the timeline (D).

(E–H) Histology and histomorphometry at the wound center on day 7 (n = 9 *Postn-Pdgfra$^{F/+}$*, 6 *Postn-Pdgfra$^{F/F}$*, and 5 *Postn-Pdgfra$^{K/+}$* mice). H&E staining. Dotted lines indicate the wound bed area (E). Wound bed cross-sectional area (F). Contraction (G).

Epithelialization (H). Data are plotted as mean ± SEM. Each point represents one mouse. Scale bars, 200 μm.

(I and J) Tomato and αSMA at the wound center on day 7. Dotted lines indicate the wound bed area. Scale bars, 200 μm.

(K and L) PCR genotyping for recombination in wounded skin (w) versus unwounded skin (u), with germline mutant DNA as positive control. SA-Flp PCR identifies Cre-mediated deletion of the PDGFRα cassette in *Postn-Pdgfra*$^{Fl/+}$ wounds (K). SA-aK PCR identifies Cre-mediated deletion of the PGKNeo cassette in *Postn-Pdgfra*$^{K/+}$ wounds (L).
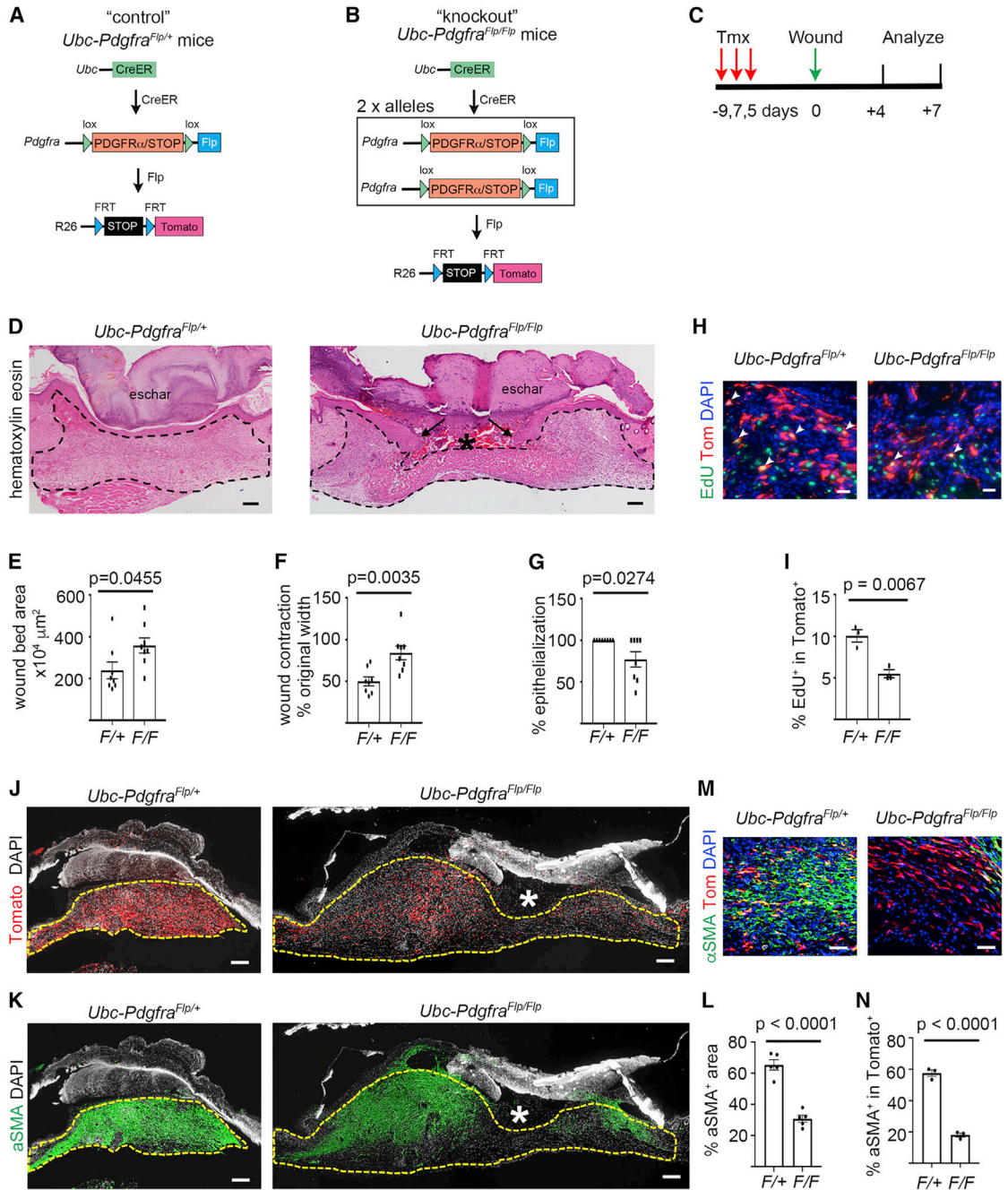
See also Figures S3 and S4.

Figure 4. PDGFRα is required for fibroblast proliferation and myofibroblast differentiation
(A–C) Schematic of the genetic labeling strategy for *Ubc-Pdgfra^{Flp/+}* control mice (A) and
Ubc-Pdgfra^{Flp/Flp} knockout mice (B) and the timeline (C).
(D–G) Histology and histomorphometry at the wound center on day 7 (n = 8 of each
genotype). H&E staining: granulation tissue has not filled the *Pdgfra^{F/F}* wound bed,
leaving a gap (asterisk) with downward migrating epithelial tongues (arrows). Dotted line
indicates the wound bed area. (D). Wound bed cross-sectional area (E). Contraction (F).
Epithelialization (G). Scale bars, 200 μm.

(H and I) EdU/Tomato co-labeling of proliferating cells on day 4. Arrowheads indicate EdU$^+$Tomato$^+$ cells (H). Quantification of EdU in Tomato$^+$ cells (n = 3 mice per genotype) (I). Scale bars, 50 μm.

(J and K) Tomato and αSMA at the wound center on day 7. Asterisk indicates tissue gap in the wound center. Dotted lines indicate the wound bed area. Scale bars, 200 μm.

(L) Quantification of αSMA$^+$ area on day 7 (n = 5 mice per genotype).

(M and N) αSMA/Tomato co-labeling on day 7 (M). Quantification of αSMA in Tomato$^+$ cells (n = 3 mice per genotype) (N). Scale bar, 50 μm. Data are plotted as mean ± SEM. Each point represents one mouse.

Note: experiments in Figures 1 and 4 were performed at the same time, so the *Fl*/+ control quantifications are the same between the two figures.
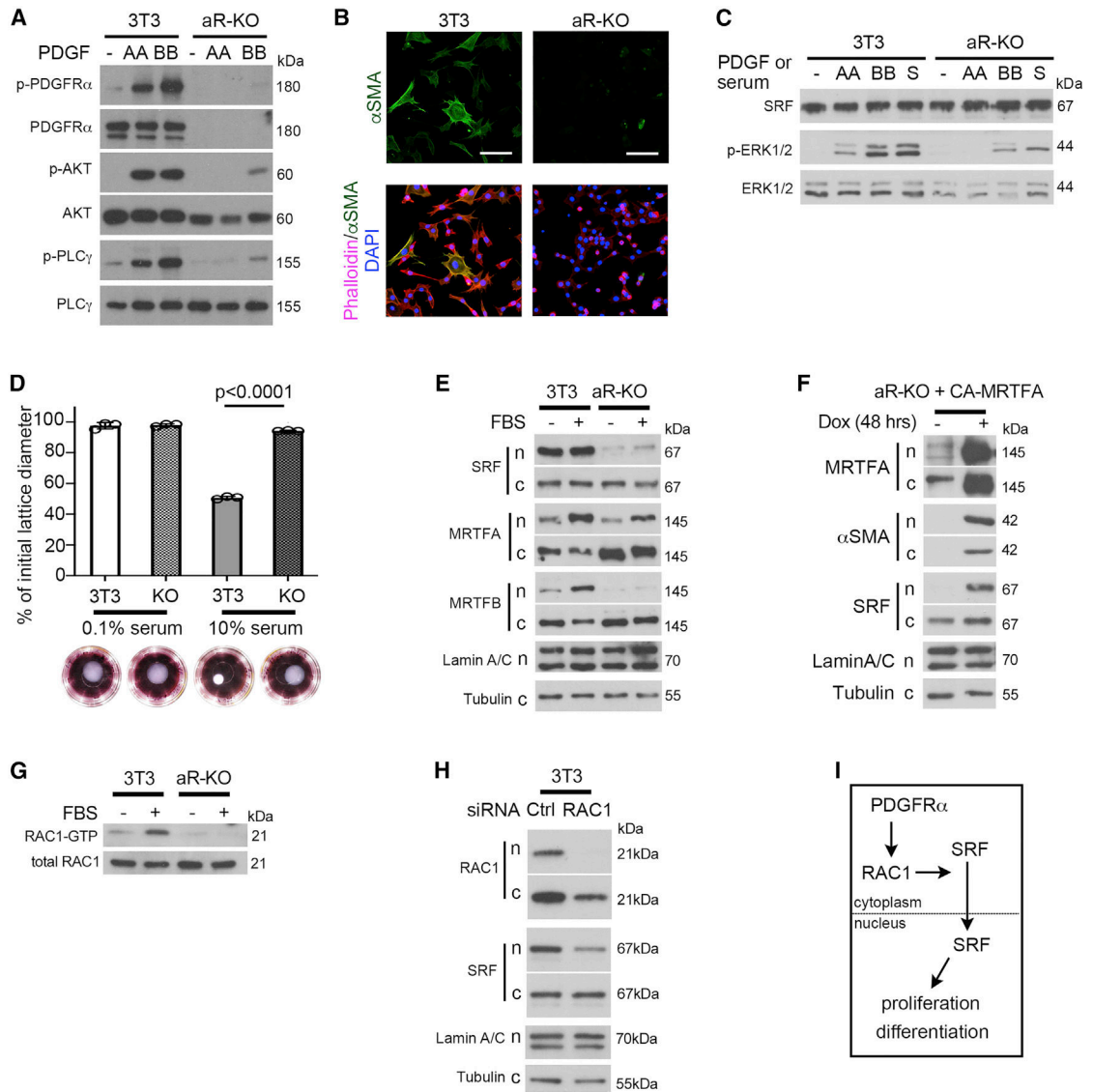
See also Figure S5.

Figure 5. PDGFRα and RAC1 regulate SRF nuclear localization.

(A–H) Wild-type 3T3 cells and 3T3 cells with Cas9-mediated *Pdgfra* knockout (aR-KO).

(A) Cells serum starved and treated with 50 ng/mL PDGF-AA or PDGF-BB for 30 min, then processed for western blot.

(B) Cells stained for F-actin and αSMA. Scale bar, 50 μm. Total SRF levels are similar between genotypes.

(D) Collagen lattice contraction, expressed as a pecentage of the initial diameter, with representative images at 24 h after lattice detachment (n = 3 biological replicates per genotype). Data are plotted as mean ± SD. Each point represents one biological replicate.

(E) Western blot with nuclear (n) and cytoplasmic (c) fractions after serum for 30 min. SRF and MRTFB are predominantly cytoplasmic in aR-KO cells.

(F) aR-KO cells with a doxycycline (dox)-inducible constitutively active (CA–) MRTFA were serum starved and treated with dox for 48 h. Western blot of nuclear (n) and

cytoplasmic (c) fractions shows that CA-MRTFA restores SRF nuclear localization and αSMA expression.

(G) aR-KO cells fail to activate Rac1 when serum starved and treated with 10% FBS for 10 min

(H) siRNA knockdown of RAC1 reduces SRF nuclear localization.

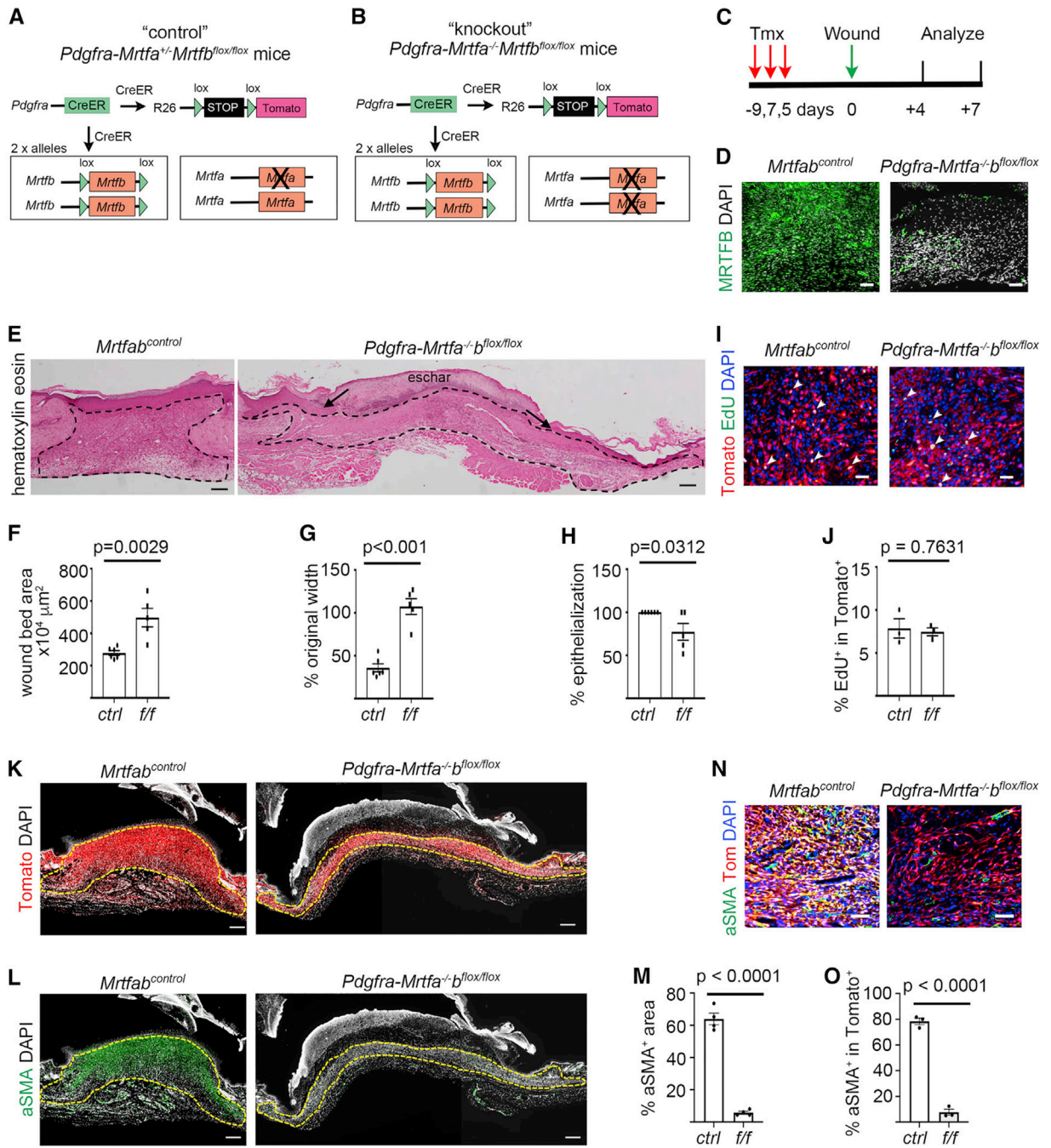(I) Summary of the proposed PDGFRα-RAC1-SRF relationship.

See also Figure S6.

Figure 6. Mrtfa/Mrtfb are required for myofibroblast differentiation but not proliferation

(A–C) Schematic of the genetic labeling strategy for *Pdgfra-Mrtfa*^{+/−} *Mrtfb*[flox/flox] control mice (A) and *Pdgfra-Mrtfa*^{−/−} *Mrtfb*[flox/flox] knockout mice (B) and the timeline (C).

(D) Stain for MRTFB in day 7 wound tissue. Scale bars, 100 μm.

(E–H) Histology and histomorphometry at the wound center on day 7 (n = 5–6 of each genotype). H&E staining: the knockout wound bed is filled with granulation tissue, but the wound is uncontracted with widely separated epithelial tongues (arrows). Dotted line indicates the wound bed area.

(E). Wound bed cross-sectional area (F). Contraction (G). Epithelialization (H). Scale bars, 200 μm.

(I and J) EdU/Tomato co-labeling of proliferating cells on day 4. Arrowheads indicate EdU[+]Tomato^{+} cells (I). Quantification of EdU in Tomato^{+} cells (n = 3 mice per genotype) (J). Scale bars, 50 μm.

(K and L) Tomato and αSMA at the wound center on day 7. Dotted lines indicate the wound bed area. Scale bars, 200 μm.

(M) Quantification of αSMA[+] area on day 7 (n = 4 mice per genotype).

(N and O) αSMA/Tomato co-labeling on day 7 (N). Quantification of αSMA in Tomato^{+} cells (n = 3 mice per genotype) (O). Scale bar, 50 μm. Data plotted as mean ± SEM. Each point represents one mouse.
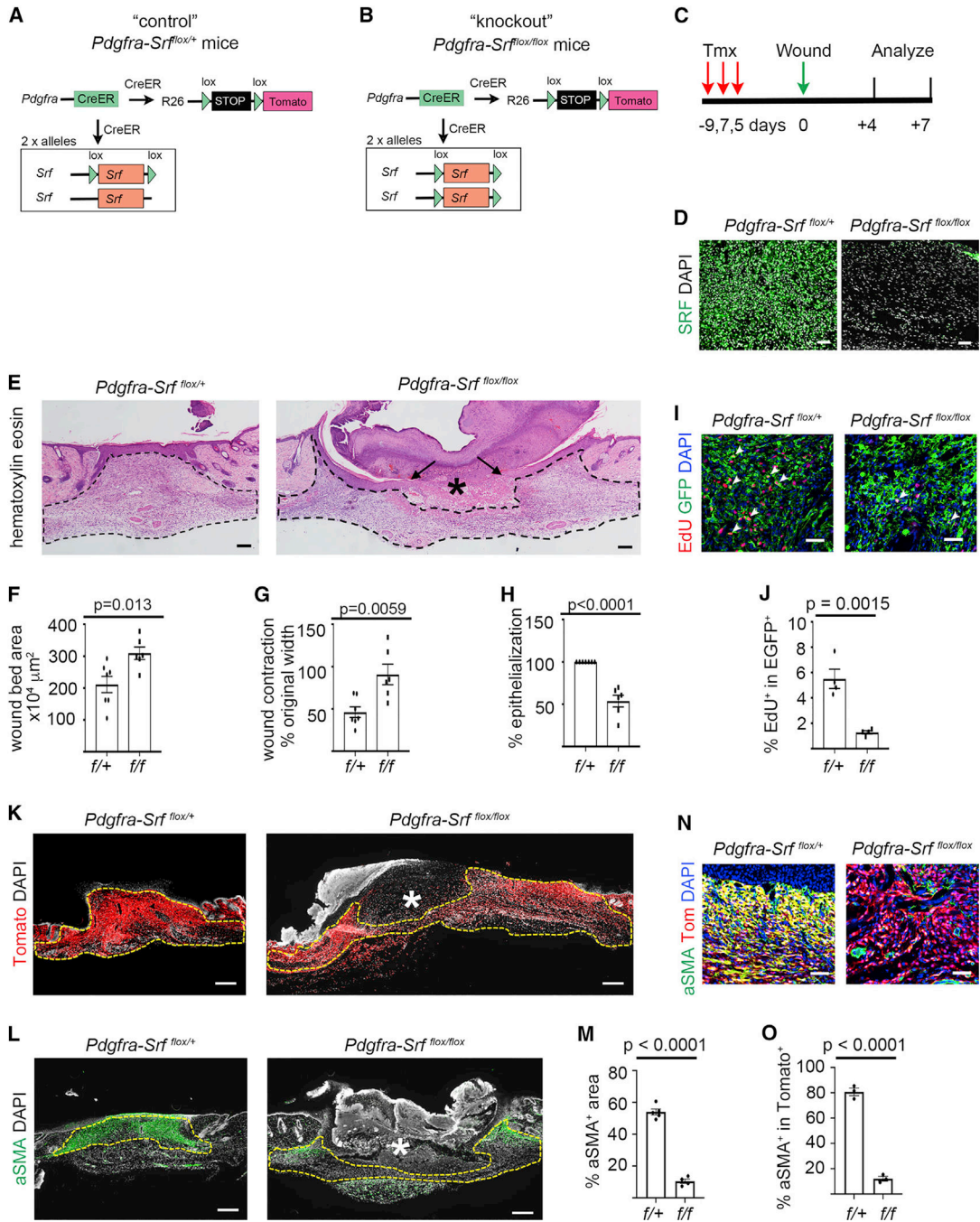
Figure 7. Srf is required for proliferation and myofibroblast differentiation

(A–C) Schematic of the genetic labeling strategy for *Pdgfra-Srf^flox/+* control mice (A) and *Pdgfra-Srf^flox/flox* knockout mice (B) and the timeline (C).

(D) Stain for SRF in day 7 wound tissue. Scale bars 100 μm.

(E–H) Histology and histomorphometry at the wound center on day 7 (n = 6–7 of each genotype). H&E staining: granulation tissue has not filled the knockout wound bed, leaving a gap (asterisk) with downward migrating epithelial tongues (arrows). Dotted line

indicates the wound bed area. (E). Wound bed cross-sectional area (F). Contraction (G). Epithelialization (H). Scale bars, 200 μm.

(I and J) Mice have a Col1a1-GFP reporter to identify fibroblasts. EdU/GFP co-labeling of proliferating cells on day 4. Arrowheads indicate EdU$^+$GFP$^+$ cells (I). Quantification of EdU in GFP$^+$ cells (n = 4 mice per genotype) (J). Scale bars, 50 μm.

(K and L) Tomato and αSMA at the wound center on day 7. Asterisk indicates tissue gap in the wound center. Dotted lines indicate the wound bed area. Scale bars, 200 μm.

(M) Quantification of αSMA$^+$ area on day 7 (n = 4–5 mice per genotype).

(N and O) αSMA/Tomato co-labeling on day 7 (N). Quantification of αSMA in Tomato$^+$ cells (n = 3 mice per genotype) (O). Scale bar, 50 μm. Data plotted as mean ± SEM. Each point represents one mouse.

See also Figure S7.

KEY RESOURCES TABLE

REAGENT or RESOURCE	SOURCE	IDENTIFIER
Antibodies		
Goat anti-PDGFRα	R&D	Cat# AF1062; RRID:AB_2236897
Rabbit anti-PDGFRα	Santa Cruz	Cat# 338; RRID:AB_631064
Rabbit anti-p-PDGFRα (Y762)	Cell Signaling	Cat 24188; RRID:AB_2798873
Rabbit anti-PDGFRβ	Santa Cruz	Cat# 432; RRID:AB_631068
Rabbit anti-p-PDGFRβ (Y1009)	Cell Signaling	Cat# 3124; RRID:AB_823455
Rabbit anti-SRF	Santa Cruz	Cat# 335; RRID:AB_2255249
Rabbit anti-Periostin	Abcam	Cat# ab14041; RRID:AB_2299859
Rabbit anti-αSMA	Cell Signaling	Cat# 19245; RRID:AB_2734735
Rabbit anti-MRTF-A	Cell Signaling	Cat# 14760; RRID:AB_2798598
Rabbit anti-MRTF-B	Cell Signaling	Cat# 14613; RRID:AB_2798539
Rabbit anti-Smad2/3	Cell Signaling	Cat# 8685; RRID:AB_10889933
Rabbit anti-p-Smad3	Rockland	Cat# 600-401-919; RRID:AB_2192878
Rabbit anti-ERK1/2	Cell Signaling	Cat# 4695; RRID:AB_390779
Rabbit anti-p-ERK1/2 (T202/204)	Cell Signaling	Cat# 4370; RRID:AB_2315112
Rabbit anti-Akt	Cell Signaling	Cat# 9272; RRID:AB_329827
Rabbit anti-Akt (S473)	Cell Signaling	Cat# 4051; RRID:AB_331158
Rabbit anti-PLCγ	Cell Signaling	Cat# 2822; RRID:AB_2163702
Rabbit anti-p-PLCγ (Y783)	Cell Signaling	Cat# 14008; RRID:AB_2728690
Rabbit anti-βTubulin	Cell Signaling	Cat# 2146; RRID:AB_2210545
Mouse anti-Lamin A/C	Cell Signaling	Cat# 4777; RRID:AB_10545756
Rabbit anti-TSC2	Cell Signaling	Cat# 4308; RRID:AB_10547134
Goat anti-RFP	Rockland	Cat# 200-101-379; RRID:AB_2744552
AF647 Phalloidin	Cell Signaling	Cat# 8940
CF594 Phalloidin	Biotium	Cat# 00045
Goat anti-rabbit biotin conjugate	Vector Labs	PK-6101; RRID:AB_2336820
Donkey anti-goat Cy3 conjugate	Jackson ImmunoResearch	Cat# 705-165-003; RRID:AB_2340411
Donkey anti-rabbit HRP conjugate	Jackson ImmunoResearch	Cat# 711-035-152; RRID:AB_10015282
Donkey anti-mouse HRP conjugate	Jackson ImmunoResearch	Cat# 715-035-150; RRID:AB_2340770
Donkey anti-rabbit AF488 conjugate	Jackson ImmunoResearch	Cat# 711-545-152; RRID:AB_2313584
Chemicals, peptides, and recombinant proteins		
Tamoxifen (Tmx)	Sigma Aldrich	Cat# T5648
Human TGFb1	Peprotech	Cat# 100-21C
Rat PDGF-BB	R&D Systems	Cat# 520-BB
Rat-PDGF-AA	R&D Systems	Cat# 1055-AA
EdU	Invitrogen	A10044
Fetal Bovine Serum	Atlanta Biologicals	S11550
Control siRNA-A	Santa Cruz	sc-37007

REAGENT or RESOURCE	SOURCE	IDENTIFIER
Rac1 siRNA (mouse)	Santa Cruz	sc-36352
Critical commercial assays		
ECL Western blotting substrate	Pierce	Cat# 32106
BCA assay	Pierce	Cat# 23225
Vectastain ABC Kit	Vector Labs	PK-6101
DAB Peroxidase Substrate Kit	Vector Labs	SK-4100
iTaq SYBR Green Supermix	Bio-Rad	Cat# 1725122
Active Rac1 Detection Kit	Cell Signaling Technology	Cat# 8815
Lipofectamine RNAiMAX	Invitrogen	13778
35 mm TPP cell culture dish	Techno Plastic Products	93040
Experimental models: Cell lines		
NIH3T3 mouse embryonic fibroblasts	(Todaro and Green, 1963)	RRID:CVCL_0594
aR-KO NIH3T3 cells	This manuscript	N/A
Experimental models: Organisms/strains		
Mouse: Ubc-CreER[tg]	(Ruzankina et al., 2007)	JAX:007001
Mouse: Pdgfra-Cre[tg]	(Rivera-Gonzalez et al., 2016)	JAX:013148
Mouse: Pdgfra[CreER]	(Chung et al., 2018)	JAX:032770
Mouse: Postn[MerCreMer]	(Kanisicak et al., 2016)	JAX:029645
Mouse: Pdgfra[H2B:GFP]	(Hamilton et al., 2003)	JAX:007669
Mouse: Col1a1-GFP[tg]	(Lin et al., 2008)	N/A
Mouse: R26[fSf-tdTomato]	(Sun et al., 2020)	N/A
Mouse: R26[LSL–Tomato]	(Madisen et al., 2010)	JAX:007914
Mouse: Pdgfra[K.Flp]	(Sun et al., 2020)	N/A
Mouse: Pdgfra[Flp]	(Sun et al., 2020)	N/A
Mouse: Srf[floxed]	(Miano et al., 2004)	JAX:006658
Mouse: Mrtfa[null]	(Mokalled et al., 2010)	N/A
Mouse: Mrtfb[floxed]	(Mokalled et al., 2010)	N/A
Oligonucleotides		
See Table S2		
Recombinant DNA		
eCas9 1.1	(Slaymaker et al., 2016)	Addgene #71814
pENTR eCas9 1.1	This manuscript	N/A
pLenti CMV Hygro DEST	(Campeau et al., 2009)	Addgene #17454
pLenti CMV eCas9 1.1 Hygro	This manuscript	N/A
pInducer 20	(Meerbrey et al., 2011)	Addgene #44012
lenti-Guide Puro	(Sanjana et al., 2014)	Addgene #52963

REAGENT or RESOURCE	SOURCE	IDENTIFIER
lenti-mm sgPDGFRα #2 Puro	This manuscript	N/A
Software and algorithms		
ImageJ	N/A	https://imagej.nih.gov/ij/
GraphPad Prism 9	N/A	N/A
Other		
LabDiet 5053 (normal chow)	Purina	LabDiet 5053